Title: Where in the leaf is intercellular CO_2 (C_i)? Considerations and recommendations for assessing gaseous diffusion in leaves

Authors: Joseph R. Stinziano[1], Jun Tominaga[1,2], David T. Hanson[1*]

Affiliations:

[1]Department of Biology, The University of New Mexico, Albuquerque, NM 87104, USA,

[2]Department of Mathematical and Life Sciences, Hiroshima University, Hiroshima 739-8526, Japan

***Corresponding author:** David T. Hanson; email: dthanson@unm.edu

Other email addresses: jstinziano@unm.edu, jtominaga@unm.edu

ORCiDs

Joseph R. Stinziano: 0000-0002-7628-4201

Jun Tominaga: 0000-0001-7338-1826

David T. Hanson: 0000-0003-0964-9335

Date of submission: May 5, 2020

Tables: 2

Figures: 8 (1-7 color) plus 5 supplemental (all color)

Word count: 10,271

Highlight

Leaf water vapor and CO_2 exchange have been successfully used to model photosynthetic biochemistry. We review critical assumptions in these models and make recommendations about which need to be re-assessed.

Abstract

The assumptions that water vapor exchange occurs exclusively through stomata, that the intercellular airspace is fully saturated with water vapor, and that CO_2 gradients are negligible between stomata and the intercellular airspace have enabled significant advancements in photosynthetic gas exchange research for nearly 60 years via calculation of intercellular CO_2 (C_i). However, available evidence suggests that these assumptions may be overused. Here we review the literature surrounding evidence for and against the assumptions made by Moss & Rawlins (1963). We reinterpret data from the literature by propagating different rates of cuticular water loss, CO_2 gradients, and unsaturation through the data. We find that in general, when cuticle conductance is less than 1% of stomatal conductance, the assumption that water vapor exchange occurs exclusively through stomata has a marginal effect on gas exchange calculations, but this is not true when cuticle conductance exceeds 5% of stomatal conductance. Our analyses further suggest that CO_2 and water vapor gradients have stronger impacts at higher stomatal conductance, while cuticle conductance has a greater impact at lower stomatal conductance. Therefore, we recommend directly measuring C_i whenever possible, measuring apoplastic water potentials to estimate humidity inside the leaf, and exercising caution when interpreting data under conditions of high temperature and/or low stomatal conductance, and when a species is known to have high cuticular conductance.

Keywords: *cuticle conductance, mesophyll conductance, photosynthetic capacity, photosynthesis, stomatal conductance, transpiration, water use efficiency*

Introduction

Nearly 60 years ago, Moss and Rawlins (1963) introduced a calculation to estimate intercellular CO_2 concentrations (C_i) under the assumption that all water flux out of the leaf occurs through the stomata. The importance of their findings was such that it quickly became dogma and is severely under-cited (<100 citations according to Google Scholar) despite underlying nearly every measurement of stomatal conductance (g_s) and C_i. C_i now plays a central role in plant gas exchange research: it is used to derive parameters for a biochemical model of leaf gas exchange through measurements of net CO_2 assimilation (A_{net}) responses to CO_2 (Farquhar *et al.*, 1980), which in turn can be used to drive photosynthesis in coupled vegetation-climate models (e.g. Oleson *et al.*, 2013), and C_i is a necessary starting point for estimating CO_2 fluxes within leaves all the way to the site of carboxylation (Evans *et al.*, 1986). However, this approach uses myriad assumptions that are generally not realistic (and almost physically impossible in other cases), including saturated vapor pressure in the leaf (Hygen, 1951, 1953; Slavik, 1958; Jarvis & Slatyer, 1970; Ward & Bunce, 1986; Egorov & Karpushkin, 1988; Karpushkin, 1994; Campbell & Norman, 1998; Canny & Huang, 2006; Cernusak et al., 2018), negligible cuticular conductance (Boyer et al., 1997; Meyer & Genty, 1998; Šantrůček et al., 2004; Boyer 2015a; Tominaga & Kawamitsu, 2015a; Tominaga et al., 2018), homogenous stomatal conductance (Downton et al., 1988; Terashima et al., 1988; Buckley et al., 1997; Meyer & Genty, 1998), no CO_2 gradients within leaves (i.e. infinite CO_2 conductance; Parkhurst, 1984; Long et al., 1989), no air pressure gradients within the leaf (Leuning, 1983; Dacey, 1987), strict Fickian diffusion of CO_2 into leaves (Leuning, 1983; Dacey, 1987), and resistances to gas diffusion are additive (i.e. follow the Ohm's law analogy, Parkhurst, 1984). For the purposes of this review, we define infinite conductance as a conductance high enough that a negligible concentration gradient forms between the two compartments in question. Here we review the concept of C_i, g_s, and assumptions inherent in their calculations, and provide recommendations on moving beyond the Moss and Rawlins (1963) paradigm of assumptions.

The Moss and Rawlins (1963) paradigm

To calculate stomatal resistance, Gaastra (1959), with Brown and Escombe's (1900) Ohm's law analogy of resistances to gas diffusion (although this may not necessarily hold true: see Parkhurst, 1984), introduced a series of Equations:

$$A_{net} = \frac{C_a - C_i}{r_{sc}} = g_{sc}(C_a - C_i) \quad \text{Eq. 1}$$

$$\mathrm{E} = \frac{W_i - W_a}{r_{sw}} = g_{sw}(W_a - W_i) \quad \text{Eq. 2}$$

where A_{net} is net CO_2 assimilation, C_a is the CO_2 concentration external to the leaf, r_{sc} and g_{sc} is the stomatal resistance and conductance (reciprocal of resistance) to CO_2, E is transpiration through the stomata, W_a and W_i are the water vapor concentration external to the leaf and in the intercellular airspace, r_{sc} and g_{sc} is the stomatal resistance and conductance to water vapor. Considering the boundary resistance was negligibly small in the measurement system (which we also assume through this review), Moss and Rawlins (1963) expressed the diffusion properties of CO_2 and water vapor in leaves as:

$$\frac{g_{sw}}{g_{sc}} = \frac{D_w}{D_c} \quad \text{Eq. 3}$$

where D_w and D_c are the diffusion coefficients for CO_2 and water vapor in air. D_w/D_c is usually assumed to be equal to ~1.6 (Li-Cor, 2019; although see Holmgren et al 1965 Physiologia Plant. 18:557 where they use 1.7). Note that 1) Massman (1998) reported a mean ratio of 1.577 with uncertainties as high as 7% for the diffusivity of water vapour, 2) the number is valid for Fickian diffusion, and 3) this may vary if the stomatal pore size is small enough that Knudsen diffusion occurs instead of Fickian diffusion (e.g. Parkhurst, 1994). Solving the system of Eqs.1-3 they obtained:

$$C_i = C_a - 1.6\left(\frac{A_{net}}{E}\right)(W_i - W_a) \quad \text{Eq. 4}$$

where W_i is assumed to be saturated for the leaf temperature (T_{leaf}). Using conductance term, Eq. 4 can be rewritten as:

$$C_i = C_a - 1.6\frac{A_{net}}{g_{sw}} \qquad \text{Eq. 5}$$

Given that C_a and A_{net} are directly measurable, g_{sw}, calculated from E and water vapor gradients (W_a-W_i) (Eq. 2), would be the critical parameter that determines validity of C_i (though measurement precision of C_a and A_{net} affects the calculation).

Based on the above, Moss and Rawlins (1963) introduced assumptions (both explicitly and implicitly) into the calculation of C_i:

1. All transpired water flows through stomata
2. No CO_2 or H_2O gradients within leaves (internal conductance, $g_{ias} = \infty$)
3. W_i is at saturation (W_i = saturation vapor pressure, e_s; mesophyll apoplast water potential, $\Psi_{m,apo} = 0$)
4. Uniform stomatal apertures over leaf surfaces
5. No air pressure gradients across leaf surfaces
6. $\frac{D_w}{D_c} = 1.6$ (based on Fickian diffusion in air)
7. One-dimensional models approximate the three-dimensional leaf

For the purposes of this review, we are going to address the data surrounding the implications and failures of assumptions 1 to 3 in relation to C_i calculations and data derived from C_i and give a cursory overview on the remaining assumptions. Note that these assumptions equally apply to the von Caemmerer and Farquhar (1981) modification to Moss and Rawlins (1963).

What do tests of Moss and Rawlins (1963) say?

The first test of the calculation was done in 1982 (Sharkey *et al.*, 1982) whereby C_i was directly measured and compared to the calculated value based on the Moss and Rawlins assumption. Sharkey *et al*. (1982) used a dual open-flow/closed-flow system

whereby one side of the leaf was equilibrated in a closed system to measure C_i, while the other side was measured with the open-flow system used to calculate C_i. Note that this method requires a steady-state setup and assumes that the CO_2 in the closed-flow system is in equilibrium with the internal airspace of the leaf. Sharkey *et al*. (1982) concluded that the calculated values were in "good agreement" with the measured values, although there were some deviations less than ±20 μmol mol^{-1} (Table 1). They also reported that at very high vapor pressure difference (VPD) and conductance less than 60 mmol m^{-2} s^{-1}, the calculated C_i increased while the measured C_i decreased. Since then, fewer than 10 studies have assessed the Moss and Rawlins (1963) assumptions (Table 1) despite the fact that it is the foundation for a broad range of research activities. These studies employed direct C_i measurements similar to Sharkey et al. (1982), except for Boyer et al. (1997). Intriguingly, most evidence suggests that there are issues in the assumptions that lead to discrepancies between measured and calculated C_i (Table 1), with explanations ranging from cuticular water loss (Boyer *et al.*, 1997), to patchy stomatal apertures (Downton et al., 1988; Terashima et al., 1988; Meyer & Genty, 1998) and intra-leaf CO_2 gradients (Sharkey et al., 1982; Mott & O'Leary, 1984; Parkhurst *et al*., 1988; Parkhurst & Mott, 1990; Parkhurst, 1994).

Assumption 1 – all water flows through stomata

Cuticular water loss is a proposed explanation for the reported discrepancies (Kirschbaum and Pearcy, 1988; Boyer *et al.*, 1997; Meyer & Genty, 1998; Boyer, 2015*a*; Tominaga & Kawamitsu, 2015a, Tominaga et al., 2018). Using hypostomatous leaves of grape (*Vitis vinifera* L.), Boyer et al. (1997) measured gas exchange through the adaxial stomata-free side while the abaxial stomatous side was sealed. In this circumstance, C_i was estimated to be near the compensation point (50 μmol mol^{-1}) with a little CO_2 flux on the cuticular side while calculations showed C_i close to C_a. As a result, the calculated C_i was larger than the actual value by over a hundred μmol mol^{-1} (astomatous side of *Vitis vinifera* in Table 1). Later, this result was reproduced in the same species (Boyer 2015b) with a direct system that reached C_a as high as several % to detect very small CO_2 fluxes through the cuticle (Boyer & Kawamitsu, 2011), as well as in passion fruits (*Passiflora edulis* Sims) (Tominaga et al., 2018). Boyer (2015b) found that the

measured C_i increased by only 2 µmol mol^{-1} above the CO_2 compensation point of 44 µmol mol^{-1} despite the large CO_2 gradients (10000 µmol mol^{-1}) across the cuticular surface, suggesting that the cuticle is an effective barrier against CO_2 diffusion. Transpiration was always greater than assimilation through the cuticle, causing cuticle conductance for water vapor (g_{cw}) to be 20-40× larger than cuticle conductance for CO_2 (g_{cc}), which is a much higher ratio than the 1.6 assumed for stomata (Eq. 3). This is likely because the pathway for CO_2 in these experiments was from the leaf airspaces through the epidermal cells and cuticle, whereas the pathway for water diffusion was from the epidermal surface through the cuticle.

Calculations (Eq. 4) consistently overestimate the C_i for the astomatous side of hypostomatous leaves (Table 1). In contrast, C_i values were in closer agreement between direct measurements and calculations in the high CO_2 tests for stomatous leaf surfaces in sunflower (*Helianthus annuus* L.) (Boyer & Kawamitsu (2011) in Table 1). It should be noted that von Caemmerer and Farquhar (1981) slightly modified Eq. 4 by including a ternary effect term that describes the hinderance of CO_2 diffusion into the leaf due to the much larger flux of H_2O out of the leaf (Eq. B18 in von Caemmerer & Farquhar, 1981), and this version is used more generally and also in Table 1. Boyer & Kawamitsu (2011) experimentally validated this modification under high C_a that enhanced the ternary effect, and thus direct measurements include this effect.

To see the cuticle effect on both leaf sides (cuticle plus stomata), Boyer (1997) recalculated C_i in the standard measurements for both sides using the cuticle conductance determined on the same leaf (*Vitis vinifera* (both sides) in Table 1). The results suggest that the cuticle effect can be substantial—C_i differential is 126 µmol mol^{-1} at 1100 µmol mol^{-1} C_a— when g_{sw} is relatively small, but only marginal—C_i differential of 3 µmol mol^{-1} at 350 µmol mol^{-1} C_a— when g_{sw} is relatively large. This conclusion was recently confirmed with direct measurements in amphistomatous sunflower leaves with stomata closed by feeding ABA (Boyer, 2015a; Tominaga & Kawamitsu, 2015a), and amphistomatous bean (*Phaseolus vulgaris* L.) leaves with low stomatal density (SD) (Tominaga et al., 2018), as summarized in Table 1. In these studies (Tominaga &

Kawamitsu, 2015a; Tominaga et al., 2018), calculation and direct measurements draw essentially the same A/C_i response curves when g_{sw} was large (g_{sw}>250 mmol m^{-2} s^{-1}) with open stomata and/or high SD. In contrast, when g_{sw} was small (g_{sw}<50 mmol m^{-2} s^{-1}) with closed stomata and/or low SD, A/C_i curves were depressed due to over-estimation of the calculated C_i. The similar depression was also confirmed with the standard open-flow measurements for both sides (Tominaga & Kawamitsu, 2015a), as was observed previously in similar ABA treatments (Downton et al., 1988; Terashima et al., 1988). Clearly, this should create a problem for interpreting gas exchange measurements. Cuticular water loss also causes calculated C_i to be lower than the actual value when CO_2 is diffusing out from the leaf as it overestimates the CO_2 transfer through stomata regardless of diffusional direction. In accordance, negative C_i differentials were found with negative A_{net} in dark, and low C_a in light (Table 1).

There are debates as to whether and when cuticular water loss would be a significant portion of water loss across the leaf (Ledford, 2017). Generally, we would expect cuticle conductance to be more significant at low values of g_{sw} as noted above (Meyer and Genty, 1998; Flexas *et al.*, 2002; Lawlor, 2002) and under heat stress where the cuticle could undergo a state change to become very permeable to water (although note that cuticular melting may not occur until temperatures >60 °C, Bargel et al., 2006). But how large is leaf cuticle conductance and water loss? Unfortunately, biologists studying cuticle properties often focus on cuticle permeance (units: m s^{-1}), which can hinder comparisons with gas exchange where conductance and flux are normally measured (units mol m^{-2} s^{-1}). A series of equations permits the calculation of conductance and flux from permeance. For conductance (Hall, 1982; Nobel, 1991):

$$g_{cw} = P_c \frac{p}{RT} \qquad \text{Eq. 6}$$

Where g_{cw} is cuticular conductance for water vapor (mol m^{-2} s^{-1}), P_c is cuticular permeance (m s^{-1}), p is atmospheric pressure (Pa), R is the universal gas constant (8.314 m^3 Pa K^{-1} mol^{-1}), and T is temperature (K). And for the flow rate of water across

the cuticle (flux, transpiration), assuming steady-state conditions (Riederer and Schreiber, 2001):

$$E_c = \frac{P_c(W_i - W_a)}{18.02} \qquad \text{Eq. 7}$$

Where E_c is cuticular transpiration (water flux) across the cuticle (mol m^{-2} s^{-1}), P_c is cuticular permeance (m s^{-1}), W_i is the water vapor concentration adjacent to the outer epidermal wall (g m^{-3}), W_a is the water vapor concentration at the leaf surface (g m^{-3}), and 18.02 is the molar mass of water (g mol^{-1}).

Cuticle permeances (m s^{-1}) available in Riederer & Schreiber (2001) were converted into g_{cw} and E_c values wherever sufficient data were available in the original papers to perform the calculations (Table 2). Mean g_{cw} calculated from Riederer and Schreiber (2001) was 0.511 ± 0.101 mmol m^{-2} s^{-1} (range: 0.015 to 5.862 mmol m^{-2} s^{-1}), while mean E_c was 15.18 ± 2.66 µmol m^{-2} s^{-1} (range: 0.46 to 134.36 µmol m^{-2} s^{-1}) (Table 2; Fig 1a). How do these g_{cw} values compare to stomatal conductance?

We compared the range in g_{cw} values above to the stomatal conductances (g_{sw}) reported in Douthe *et al.* (2011), Vrábl *et al.* (2009), and Scafaro *et al.* (2011) (which we also use to test the implications of g_{cw} on mesophyll conductance, g_m, below; see Pons et al., 2009 for a discussion of this). Given that measured g_{sw} from the studies used for the g_m analysis varied from 43.6 to 1,253 mmol m^{-2} s^{-1} (mean: 474 ± 44 mmol m^{-2} s^{-1}), a quick estimate suggests that g_{cw} could range between 0.001 and 13% of g_{sw} measurements (calculation based on means: 0.1% of g_{sw}), which may have significant implications for gas exchange measurements in certain species under some conditions.

Analyzing Eq. 7, there are two unknowns (P_c and W_i, though P_c is measurable in astomatous cuticles), necessitating an assumption about the value of either P_c or W_i. Typically, W_i is assumed to be equal to the water vapor concentration of the saturation vapor pressure at T_{leaf}. However, it is difficult to assess whether this assumption holds, as the site of evaporation for cuticle conductance is within the cell wall of the epidermis

and reflects a different site of evaporation than for airspace W_i. This assumption may be broken during the dry-down experiments for gravimetrically-determined cuticular water loss. During these measurements, water loss rates decline over time until a breakpoint and a constant rate of water loss are achieved. Beyond the breakpoint, stomata are assumed to be closed. Furthermore, despite the leaf having lost a substantial amount of water, the W_i assumption is used to calculated P_c, with W_i assumed to be the same for the cell wall of the epidermis and the intercellular airspace. Therefore, at a given value of E_c, when the W_i assumption is violated, then P_c will change. In this way, it is possible that much of the literature on cuticular water loss is mis-estimating cuticular permeances, and therefore cuticular conductance. This could explain why gas exchange estimates of cuticular conductance often far exceed the conductance measured using the gravimetric method or isolated cuticles, although leaky stomata in the gas exchange methods could contribute to these differences as well.

Assumption 2 – no CO_2 or H_2O gradients within leaves

Due to finite intercellular CO_2 conductance in leaves (g_{ias}), adaxial-abaxial gradients of C_i must exist along the mesophyll cells (CO_2 sink). In amphistomatous leaves, CO_2 diffuses through stomata on both sides, and the diffusion path meets somewhere in the middle of the leaf where the gradient ends. Because CO_2 diffuses slowly through cuticle, larger C_i gradients would develop in hypostomatous leaves than in amphistomatous leaves as the path-length could be longer in the airspace (Parkhurst and Mott, 1990; Evans and Loreto, 2000). Direct measurement technically alters amphi- to hypostomatous leaves by closing one surface, thereby doubling the diffusion path (e.g., Fig. 9 in Boyer & Kawamitsu, 2011). While CO_2 is entering through one side, direct measurements measure the CO_2 equilibrated at the opposite side—end of the diffusion path—and thus measures the lowest C_i for the gradient. Therefore, positive C_i differentials observed in amphistomatous leaves may be associated with the gradient. Parkhurst et al. (1988) explored this effect by observing 20-60 μmol mol^{-1} C_i differentials at about ambient 300-350 μmol mol^{-1} CO_2 in five amphistomatous species (Table 1). Considering the differential as the C_i gradient, they estimated the difference between calculated C_i and mean C_i to be 1/6 of the gradient or 3-10 μmol mol^{-1} for these

amphistomatous species, according to the one-dimensional diffusion analysis. Their estimation depends on the location of calculated C_i which, in turn, depends on the diffusion path for water vapor because calculations assume the same pathway for CO_2 and H_2O in stomatal conductance. The diffusion path for stomatal conductance is then defined by the point where the gradients of water vapor starts (i.e. the conceptual evaporating surface), that is W_i (Eq. 2). Parkhurst et al. (1988) and Sharkey et al. (1982) considered this was right beneath stomata or stomatal cavity. However, this may not be true due to water vapor gradients and/or unsaturation of water vapor in the leaf airspace (see below). For the C_i differentials they observed, cuticle conductance might have an impact especially when stomatal conductance was small, yet they did not report g_{sw} (Table 1).

Dual sided open-flow data on amphistomatous leaves suggest that CO_2 concentrations gradients are minimal across the leaf surface (Mott & O'Leary, 1984), however it is important to note that these data relied on the assumption that W_i is saturated at the substomatal cavity. Calculations for C_i are at the physical evaporating surfaces (W_i), which is not necessarily in the substomatal cavity. Therefore, such data do not provide evidence against a CO_2 concentration gradient *per se*, but rather that the CO_2 concentration gradient is less than that required to cause a substantial difference between [CO_2] at the evaporating surfaces on the adaxial and abaxial sides of the leaf.

As mentioned above, location of W_i is critical to define location of C_i through altering the diffusion path(-length) for stomatal conductance as illustrated in Fig. 2a. In general, W_i is considered to be saturated at T_{leaf} or 100% relative humidity (RH) throughout the airspace up until sub-stomatal cavity (shown as 100 in Fig. 2a). In this representation, calculated C_i is at the sub-stomatal cavity ($C_{i,s}$), and the $C_{i,s}$ is further reduced toward the mesophyll cell surface ($C_{i,ias}$) due to finite g_{ias}. When leaves are transpiring through stomata, evaporation essentially occurs on the cell surfaces exposed to the intercellular airspace (e.g., apoplast of the mesophyll cells). As for assimilation, a W_i gradient must exist from the evaporating surface to the stomatal cavity due to finite conductance to water vapor (shown as blue gradient on left hand side of Fig. 2a). In such case, the

calculated C_i would be closer to the mesophyll cell surfaces where 100% RH occurs (i.e., $C_{i,ias}$).

Assumptions 3 – W_i saturation and $\Psi_{m,apo}$ = 0 MPa

Besides W_i gradients, water potential of the water on the evaporating surface of the apoplast of the mesophyll cells ($\Psi_{m,apo}$, the location most pertinent to C_i) would affect the location of saturated W_i because RH over a solution is a function of Ψ of the solution as (Campbell & Norman, 1998):

$$RH = exp\left(\frac{M_w \psi}{RT}\right) \qquad \text{Eq. 8}$$

where M_w is the molecular weight of water (0.018 kg mol^{-1}), Ψ is the water potential in J kg^{-1} (numerically equivalent to kPa), R is the universal gas constant (8.314 J K^{-1} mol^{-1}), and T is the temperature in K. Eq. 8 indicates that RH in the airspace decreases as the $\Psi_{m,apo}$ declines. If we assume that apoplastic and symplastic water potentials are in equilibrium in leaves, bulk water potential in leaf tissue (Ψ_{leaf}), which we normally measure, may approximate the Ψ_{apo}. We note that it is the water potential at the mesophyll apoplast that matters most for C_i calculations that are relevant for photosynthetically active tissues. Water potential of the bulk apoplast (Ψ_{apo}) is composed of both mesophyll and bundle sheath apoplastic components ($\Psi_{m,apo}$ and $\Psi_{b,apo}$), and thus may be insufficient for calculating W_i. However, the importance of this depends on the ratio of mesophyll to bundle sheath. If we assume that the bundle sheath + epidermal transpiration is small relative to mesophyll transpiration, then we can assume that $\Psi_{apo} \approx \Psi_{m,apo}$.

However if we assume for a moment that $\Psi_{leaf} = \Psi_{apo}$, and $\Psi_{m,apo}$ is the relevant value for calculating W_i, for a leaf at night, Ψ_{leaf} can be as high as -0.1 MPa, corresponding to a W_i that is 99.9% RH, while a leaf at daytime with a Ψ_{leaf} of -2.0 MPa corresponds to a W_i of 98.5% RH (Eq. 8). Martínez-Vilalta et al. (2014) compiled a global dataset of water potential measurements, finding median predawn Ψ_{leaf} of -0.69 MPa (mean: -0.111 MPa, IQR: -0.13 – -0.34 MPa) and midday Ψ_{leaf} of -1.72 MPa (mean: -2.05 MPa, IQR: -

2.41 MPa – -1.23 MPa) corresponding to 99.5% (mean: 99.2%, IQR: 99.1 – 99.8 %) RH at predawn (assuming leaf temperatures of 25 °C) and 98.8% (mean: 98.5%, IQR: 98.3 – 99.1%) RH at midday. The effect of unsaturation on the calculation is illustrated on right hand side of Fig. 2a. 100% RH no longer exists in the intercellular airspace. Instead, it is located an imaginary point within the mesophyll cell ($C_{i,liq}$), thereby causing the calculated C_i to be lower than the actual C_i in the airspace.

Some studies have suggested that the airspace could be unsaturated (Hygen, 1951, 1953; Slavik, 1958; Jarvis & Slatyer, 1970; Ward & Bunce, 1986; Egorov & Karpushkin, 1988; Karpushkin, 1994; Canny & Huang, 2006; Cernusak *et al*., 2018, 2019), while others have considered that effect of the Ψ_{leaf} is so small that the 100% RH can be assumed (Farquhar & Raschke, 1978; Jones & Higgs, 1980; Sharkey *et al*., 1982; Parkhurst et al., 1988; Buckley et al. 2017, Buckley and Sack 2019). However, Cernusak et al. (2018) recently estimated that the relative humidity could be as low as 77% and 87% ($\Psi \approx -35$ MPa and –18 MPa, respectively) in *Pinus edulis* and *Juniperus monosperma* when the leaves opened stomata and actively photosynthesized. If true, unsaturation can have significant impact on the calculations at least in those species.

Assumption 4 – uniform stomatal apertures over leaf surfaces

Non-uniform stomatal apertures or stomatal 'patchiness' is another factor that could bias calculation of C_i (Downton et al., 1988; Terashima et al., 1988). They found patchy distribution of A_{net} throughout the leaves fed with ABA and proposed that if it is associated with stomatal patchiness, C_i would vary among patches and averaged C_i would be overestimated based on the conductance-weighed calculation (Eq. 5; Mansfield et al., 1990; Terashima, 1992; Buckley et al., 1997). Patchiness likely occurs in plants under water stresses that induce stomatal closure, however it is not a general phenomenon as it appears to depend on species, growth conditions, and how quickly the stress is imposed (Cheeseman 1991, Gimenez et al., 1992; Gunasekera & Berkowitz, 1992; Wise et al., 1992; Tezara et al., 1999; Mott & Buckley, 2000). A number of methods have been used to assess patchiness in conjunction with gas exchange measurements (Terashima, 1992): starch accumulation (Terashima et al.,

1988), autoradiography of fixed $^{14}CO_2$ (Downton et al., 1988a,b; Gunasekera & Berkowitz, 1992; Sharkey & Seemann, 1989; Wise et al., 1992), fluorescence imaging (Daley et al., 1989; Mott, 1995; Meyer & Genty, 1998). Although the results often have been attributed to patchy stomatal closure, these methods depend on photosynthetic metabolism and could as well reflect non-uniform metabolism (Lauer & Boyer, 1992; Wise et al., 1992). Also, lateral CO_2 diffusion and different stomatal behavior on both surfaces in amphistomatous leaves should affect the extent of observed patchiness. More independent and direct measurements of aperture/g_{sw} distributions, such as direct observations (Laisk et al., 1983; Van Gardingenet al., 1989; Lawson et al., 1997) and thermal imaging (West et al., 2005; McAusland et al., 2013), may be preferable. The problems associated with stomatal patchiness are also attributable to T_{leaf} distributions that are difficult to measure accurately and are needed for W_i. Direct C_i measurement can avoid these effects as it does not rely on conductance (Lauer & Boyer, 1992; Boyer & Kawamitsu, 2011).

Assumption 5 – no pressure gradients across leaf surfaces

Pressure gradients across the leaf surface would have direct impact on the concentration gradients because same atmospheric pressure is assumed for both inside and outside the leaf. There is evidence that humidity- and thermal- induced pressure gradients can exist across leaves, with data suggesting that this is the case in *Nelumbo* (Leuning, 1983; Dacey 1987) and *Nuphar lutea* (Dacey, 1981), however such pressure gradients may be associated most closely with aquatic plants (Steinberg, 1996). A modeling analysis suggests that intercellular airspace could be pressurized by up to 4 kPa—3.9% of 101.3 kPa for standard atmosphere—across the leaf (e.g. Steinberg, 1996), and that pressure gradients should increase with saturation of the intercellular airspace. If such pressurization can occur in terrestrial plants (which could happen under low g_{ias} values and increasing radiation loads as suggested by Steinberg, 1996), the possibility exists, therefore, that while W_i may not be equal to e_s *per se*, it may equal e_s at ambient air pressure if the leaf is pressurized and leaf RH < 100%, and or exceed the expected e_s if leaf RH is close to or greater than 100%. W_i calculated with the external ambient pressure would be lower than the actual W_i inside the leaf (i.e., the

416 actual W_i is greater than 100% RH). To our knowledge, however, there are no studies
417 demonstrating leaf to air pressure gradients in terrestrial plant species.
418
419 *Assumption 6 – Fickian diffusion of CO_2 and H_2O*
420 In the case of pressure gradients across the leaf in aquatic plants, the pressure
421 gradients can be established because pore sizes are small enough that Knudsen
422 diffusion is dominant over Fickian diffusion (Steinberg, 1996). Thus, it is possible that in
423 some terrestrial species, the pore sizes could be sufficiently small as to cause Knudsen
424 diffusion to occur, altering the diffusivity constants for CO_2 and H_2O, although stomatal
425 pore size would need to be quite small for this effect (e.g. < 1 μm, Leuning, 1983), and
426 the ratio of Knudsen diffusion coefficients for H_2O and CO_2 would be 1.56 as the ratios
427 are dependent on pore size and molecular mass. Thus, while Knudsen diffusion may
428 occur in some cases, the assumption of Fickian diffusion is likely sufficient for terrestrial
429 plants in most cases.
430
431 *Assumption 7 – one dimension approximates the three-dimensional leaf*
432 The equations used in gas exchange are typically one dimensional, and it is generally
433 assumed that this is sufficient to capture the behaviour of the leaf area measured
434 through gas exchange. However, this may be insufficient (Parkhurst, 1977) and three-
435 dimensional models predict that some gas exchange traits could be strongly affected
436 (Parkhurst, 1994; Earles et al., 2018). Furthermore, three dimensional models predict
437 mechanisms behind some of the responses observed in mesophyll conductance to CO_2
438 (g_m) (Tholen & Zhu, 2011).
439
440 Implications of broken assumptions – where is C_i?
441 Most of the assumptions listed above essentially relate to meaning of stomatal
442 conductance—source of transpiration, diffusion path, behavior and diffusive capacity of
443 stomata. While cuticular CO_2 movement is very small and probably negligible in A_{net}
444 considerable cuticular water loss occurs in transpiration, and so g_{sw} should include g_{cw}.
445 Because stomatal and cuticular transpiration occur in parallel cuticle conductance is
446 additive to stomatal conductance as (Fig. 2a):

$g_{sw} = g_{sw}' + g_{cw}$ Eq. 9

where g_{sw} is what we calculate according to Eq. 2 where E includes stomatal and cuticular transpiration whereas g_{sw}' accounts for only stomatal transpiration. Eq. 9 shows that the g_{sw} is overestimated by g_{cw} (Fig. 2a). Also, the effect of g_{cw} on the calculation is expected to be greater with the larger g_{cw} and smaller g_{sw}', both of which increase the proportion of g_{cw} to g_{sw}.

Parkhurst (1994) and co-workers suggested C_i as we calculate it is better represented by $C_{i,s}$ for C_i at the stomatal cavity based on the calculations used (Fig. 2a). Parkhurst (1994) predicted that the degree of C_i over-estimation relative to the average C_i would be greater for hypostomatous leaves rather than amphistomatous leaves, and further argues that even dual-sided gas exchange measurements can only measure $C_{i,s}$, the average C_i. However, calculated C_i could be deeper than they assumed. Diffusion path of g_{sw} affects location of C_i and is potentially complicated because where a W_i gradient occurs and where W_i is saturated (100% RH) might change with microenvironment and water status in leaves. To disentangle these effects, it is helpful to find 100% RH within the leaf because it defines the starting point of g_{sw} as well as the end point of g_{sc} which sets the location of C_i. In Fig. 2a, stomatal conductance to CO_2 (g_{sc}) for each C_i site as well as W_i are indicated.

When there is no W_i gradient and the $\Psi_{m,apo}$ is zero, sub-stomatal cavity may be saturated (center of Fig. 2a). In this scenario, C_i would be calculated as $C_{i,s}$ with the g_{sc} accounting only stomatal path ($g_{sc} = g_{sc}'$). We note that the substomatal cavity may not be saturated if the cuticle extends into the substomatal cavity as it does for *Tradescantia virginiana* (Nonami et al. 1991). When the W_i gradients exist and the Ψ is zero, 100% RH may be found at the mesophyll cell surface (left hand side of Fig. 2a). Now, the calculated C_i would indicate the $C_{i,ias}$ with the g_{sc} accounting for the stomatal plus intercellular pathway from the stomatal cavity to the mesophyll cell surface ($\frac{1}{g_{sc}} =$

$\frac{1}{g_{sc'}} + \frac{1}{g_{ias}}$). When the $\Psi_{m,apo}$ is negative (right hand side of Fig. 2a), 100% RH may be within the mesophyll cell. In this case, the g_{sc} partially includes CO_2 diffusion path in the liquid phase in addition to the air phase ($\frac{1}{g_{sc}} = \frac{1}{g_{sc'}} + \frac{1}{g_{ias}} + \frac{1}{g_{liq}}$), and the C_i would be calculated as $C_{i,liq}$. The $C_{i,liq}$ would be located in the liquid path from the cell wall surface ($C_{i,ias}$) to chloroplast stroma (C_c) depending on where the assumed W_i is located. Importantly, g_{ias} and g_{liq} usually resides in the mesophyll conductance (g_m) as (Evans et al., 2009):

$$\frac{1}{g_m} = \frac{1}{g_{ias}} + \frac{1}{g_{liq}} \qquad \text{Eq. 10}$$

where g_m is defined as:

$$g_m = \frac{A_{net}}{C_i - C_c} \qquad \text{Eq. 11}$$

Clearly, g_m is affected by g_{cw} and W_i which break the assumptions of $g_{sc} = g_{sc'}$ (i.e., $C_i = C_{i,s}$, the C_i in the substomatal cavity). If g_{ias} is included in g_{sc} when saturated W_i occurs at the mesophyll cell surface, calculated C_i would be $C_{i,ias}$ rather than $C_{i,s}$ and g_m might be calculated to be strictly liquid-phase conductance ($g_m = g_{liq}$). Furthermore, some portion of g_{liq} is mis-assigned to g_{sc} as the Ψ_{apo} 'pulls' the $C_{i,liq}$ deeper into the mesophyll cells (g_{liq} error in Fig. 2b). Consequently, decreasing the path-length for CO_2 overestimates the apparent g_m (Eq. 10. Even if sub-stomatal W_i is saturated, the vapor pressure difference between air and leaf (VPD_{leaf}) may 'push' the W_i deeper into the airspace by making the W_i gradients steeper (Fig. 2c). Then, g_m would also be overestimated by reducing some portion of path-length in the airspace (g_{ias} error in Fig. 2c). These 'pushing' and 'pulling' effect can happen either independently or simultaneously or in coordinated manner when environmental water demand is excessive (e.g., under drought). We can see by this illustration that only under very specific circumstances can our current assumptions about W_i provide us with 'true' g_s, C_i, and g_m.

In the following sections, we model the implications when some of these assumptions fail, reinterpret data from the literature in several case studies on mesophyll conductance and the photosynthetic CO_2 response, and propagate different rates of cuticular water loss, W_i gradients, and unsaturation through the data.

Modeling the implications of cuticle conductance

Re-calculations of C_i, intrinsic water use efficiency, mesophyll conductance

Analogous to Eq. 5, C_i was recalculated ($C_{i,cuticle}$) with the actual g_{sw}' in Eq. 9 as:

$$C_{i,cuticle} = C_a - 1.6\frac{A_{net}}{g_{sw}'} = C_a - 1.6\frac{A_{net}}{g_{sw}-gcw} \qquad \text{Eq. 12}$$

For C_a, we assumed infinite boundary layer conductance as most papers do not report enough information to recalculate or extract boundary layer conductance and gas exchange chambers are designed to minimize boundary layers. In Eq. 12, we also assumed that cuticle conductance for CO_2 was negligible (g_{cc} = 0) because the effect of the g_{cc} on the A_{net} has been often undetectably small under experimental C_a levels (Boyer et al., 1997; Tominaga et al., 2018).

To propagate g_{cw} through the modeling, we fixed g_{cw} as a proportion of stomatal conductance (0, 1 x 10^{-5}, 1 x 10^{-4}, 1 x 10^{-3}, 1 x 10^{-2}, 5 x 10^{-2}, 1 x 10^{-1}, and 2.5 x 10^{-1}) at the lowest light intensity for light response curves (see below), 25 °C for temperature response curves (see below), and 400 µmol mol^{-1} CO_2 for the CO_2 response curves (see below).

Introducing g_{cw} into a gas exchange approach to plant water balance has implications for how we define water use efficiency, as we can partition out stomatal and cuticular water use efficiencies. By separating out cuticle and stomatal water loss components, we can better understand the immediate cause as to why plants vary in water use efficiency (i.e. stomatal versus cuticular components). This partitioning could then be

used to inform crop breeding for further enhancing water use efficiency. We recalculated intrinsic water use efficiency (*iWUE*) as:

$$iWUE_s = \frac{A_{net}}{g_{sw'}} \qquad \text{Eq. 13}$$

where $iWUE_s$ is intrinsic stomatal water use efficiency, (μmol CO_2 mol^{-1} H_2O). To calculate the effects of including cuticular conductance on water use efficiency, we used a representative steady-state A-C_i curve for *Populus deltoides* from Stinziano *et al*. (2017) and we propagated g_{cw} as a proportion of g_{sw} at a reference [CO_2] of 400 μmol mol^{-1}. For this propagation, we recalculated g_{sc} according to the standard procedure (Li-Cor, 2019):

$$g_{sc} = \frac{1}{(1+K)\left(\frac{1.6}{g_{sw}}\right)+\frac{1.37}{g_{bw}}} + \frac{K}{(1+K)\left(\frac{1.6}{g_{sw}}\right)+K\frac{1.37}{g_{bw}}} \qquad \text{Eq. 14}$$

where K is the ratio of stomata on the adaxial to the abaxial surface of the leaf (assumed to be equal to 1), and g_{bw} is the boundary layer conductance to water. Accounting for cuticular conductance in the calculations of water use efficiency leads to an increase of up to 20% in iWUE when cuticular conductance is high (Fig. 3).

Implications of cuticular conductance on the interpretation of mesophyll conductance data

g_m Calculations

Since C_c is also dependent on C_i, we need to set out *a priori* predictions of how changes in C_i would affect C_c. To predict this effect, we started with the equation describing the online isotope discrimination from (Farquhar *et al.*, 1982) as modified by (Wingate *et al.*, 2007):

$$^{13}\Delta = a_b\frac{C_a-C_s}{C_a} + a\frac{C_s-C_i}{C_a} + (b_s+a_w)\frac{C_i-C_c}{C_a} + b\frac{C_c}{C_s} - f\frac{\Gamma_*}{C_a} - (e+e^*)\frac{R_d}{kC_a} \qquad \text{Eq. 15}$$

where $^{13}\Delta$ is the predicted net ^{13}C discrimination, a_b is the ^{13}C fractionation due to diffusion through the boundary layer, a is the ^{13}C fractionation due to diffusion through the stomata, b_s is the ^{13}C fractionation due to CO_2 solubilization, a_w is the ^{13}C fractionation during diffusion in water, b is net ^{13}C fractionation during carboxylation by rubisco and PEP carboxylase, f is the ^{13}C fractionation due to photorespiration, e is the ^{13}C fractionation due to decarboxylation, e^* is apparent ^{13}C discrimination during decarboxylation, k is carboxylation efficiency, Γ_* is the photorespiratory CO_2 compensation point, and R_d is the rate of respiration in the dark. Note that for the sake of simplicity, we ignore all ternary interactions here (Farquhar and Cernusak, 2012) as it becomes an unnecessarily complex for demonstrating the reliance of g_m on C_i for this review (see below). We can rearrange this for C_c to obtain:

$$C_c = \frac{C_a\left(^{13}\Delta - a_b\right) + C_s(a_b - a) + C_i(a - b_s - a_w) + (e + e^*)\frac{R_d}{k} - f\Gamma_*}{b - b_s - a_w} \quad \text{Eq. 16}$$

Now suppose we have $C_{i,standard}$ and $C_{i,cuticle}$, and want to calculate the difference between $C_{c,standard}$ (C_c determined without g_c) and $C_{c,cuticle}$. By calculating the difference, most terms in the above Eq. cancel out (even the term with k, which should be the same in theory; see Appendix A for details), leaving us with:

$$C_{c,standard} - C_{c,cuticle} = \frac{a - b_s - a_w}{b - b_s - a_w}\left(C_{i,standard} - C_{i,cuticle}\right) \quad \text{Eq. 17}$$

Which can be further rearranged to:

$$\frac{C_{c,standard} - C_{c,cuticle}}{C_{i,standard} - C_{i,cuticle}} = \frac{a - b_s - a_w}{b - b_s - a_w} \quad \text{Eq. 18}$$

In this way, the difference in C_c can be calculated using a ratio of fractionation constants and the difference in C_i. Since a is typically assumed to be 4.4 ‰, b_s is assumed to be 1.1 ‰ at 25 °C (Vogel, 1980), a_w is assumed to be 0.7 ‰, and b is assumed to be between 27 and 30 ‰, then the difference in C_c values should be between 9.2 and 10.3

% of the difference in C_i values at 25 °C. For the g_m calculations, we took a conservative approach and assumed that the difference in C_c was 9.2% of the difference in C_i values.

Including the ternary effects from Farquhar and Cernusak (2012) makes *a priori* predictions of the effect of cuticle conductance on C_c more difficult. Describing the discrimination:

$$^{13}\Delta = \frac{1}{1-t}\left[a_b\frac{C_a-C_s}{C_a} + a\frac{C_s-C_i}{C_a}\right] + \frac{1+t}{1-t}\left[\left(b_s + a_w\right)\frac{C_i-C_c}{C_a} + b\frac{C_c}{C_s} - f\frac{\Gamma^*}{C_a} - (e+e^*)\frac{R_d}{kC_a}\right] \quad \text{Eq. 19}$$

Where t is the ternary term described by:

$$t = \frac{\left[1+\frac{a_b(C_a-C_s)+a(C_s-C_i)}{C_a-C_i}\right]}{2g_{ac}}E_s \quad \text{Eq. 20}$$

Where g_{ac} is the total conductance to CO_2 diffusion. Note that C_i, E_s, and g_{ac} all need to be corrected for g_{sw} and g_c occurring in parallel. Since g_c affects nearly every component of t, calculations using ^{13}C discrimination may be highly sensitive to g_c when considering ternary interactions. However, if we assume a C_a of 400 μmol mol^{-1}, g_{bw} of 2 mol m^{-2} s^{-1}, g_{sw} of 0.15 mol m^{-2} s^{-1}, leaf-to-air vapor pressure deficit of 1.0 kPa, A_{net} of 15 μmol m^{-2} s^{-1}, t changes value from 2.6547 in the case of no cuticle conductance up to 2.659 in the case where 10% of g_{sw} is attributed to cuticle conductance. Thus, the ternary calculations may be minimally sensitive to cuticle conductance. We can rearrange Eq. 20 for C_c:

$$C_c = \frac{a\frac{C_s-C_i}{C_a(1-t)} - a_b\frac{C_s}{C_a(1-t)} - (e+e^*)\frac{R_d(1+t)}{kC_a(1-t)} - f\frac{\Gamma^*(1+t)}{C_a(1-t)} + \frac{C_i(1+t)(b_s+a_w)}{C_a(1-t)} + \frac{a_b}{1-t} - {}^{13}\Delta}{\frac{(1+t)(b_s+a_w)}{C_a(1-t)} - \frac{b(1+t)}{C_s(1-t)}} \quad \text{Eq. 21}$$

We can see that the effect of cuticle conductance affects nearly every term in the equations. And solving for the difference between C_c without cuticle conductance ($C_{c,s}$) and with cuticle conductance ($C_{c,c}$) we get (See Appendix B for derivation):

$$C_{c,s} - C_{c,c} = \frac{a\left[(C_s - C_{i,s})(1+t_c) - (C_s - C_{i,c})(1+t_s)\right] + \left[a_b C_a - a_b C_s - 2^{13}\Delta C_a\right][t_c - t_s] + (b_s + a_w)(1+t_s)(1+t_c)\left[C_{i,s} - C_{i,c}\right]}{(1+t_s)(1+t_c)\left[b_s + a_w - \frac{bC_a}{C_s}\right]}$$

Eq. 22

where $C_{i,s}$ is C_i without cuticle conductance, $C_{i,c}$ is C_i accounting for cuticle conductance, t_s is the ternary equation without cuticle conductance, and t_c is the ternary equation with cuticle conductance. For the purposes of this review, however, we have not included the ternary effects into our modeling.

Reinterpreting gm data

We reinterpreted g_m by propagating a g_{cw} into the g_{sw} data through recalculating C_i from Eq. 12 and gm from Eq. 11. We fixed g_{cw} as a proportion of stomatal conductance (0, 1 x 10^{-5}, 1 x 10^{-4}, 1 x 10^{-3}, 1 x 10^{-2}, 5 x 10^{-2}, 1 x 10^{-1}, and 2.5 x 10^{-1}) at the lowest light intensity for light response curves (see below), 25 °C for temperature response curves (see below), and 400 µmol mol^{-1} CO_2 for the CO_2 response curves (see below).

For reinterpreting the g_m temperature response data from Scafaro et al. (2011), we included temperature response functions of g_{cw} obtained from Riederer and Schreiber (2001) fitting an Arrhenius equation on either side of the breakpoint in the Arrhenius plot:

$$g_{cw} = g_{cw,base} e^{\frac{E_a(T-298)}{298RT}}$$

Eq. 23

where $g_{cw,base}$ was determined as above, the highest and lowest E_a (25,215 J mol^{-1} with a breakpoint at 35 °C to 85,171 J mol^{-1}; 20,145 J mol^{-1} with a breakpoint at 30 °C to 69,856 J mol^{-1}, respectively) from Riederer and Schreiber (2001) were used, T is the leaf temperature in K, and R is the universal gas constant (8.314 J mol^{-1} K^{-1}). For g_m light response data, we calculated g_{cw} based on the g_a data from the lowest light intensity to minimize issues with g_{cw} exceeding g_a. In nearly all cases, g_{cw} substantially affected g_m, with notable changes occurring when g_c exceeds ~1% of g_s (Fig. 4b, d, f). In regard to environmental responses of g_m, light and temperature responses are much

more sensitive to g_{cw} than CO_2 response (Fig. 4b, d, f). It is important to note that g_m appears most sensitive to g_{cw} for C_i < 500 µmol mol^{-1}.

Reinterpreting A-C_i data

We used a representative steady-state A-C_i response from *Populus deltoides* (Stinziano *et al.*, 2017). A-C_i data were recalculated by assuming: 1) constant g_{cw} across all C_i, and 2) g_{cw} was 0 to 25% (in increments of 0.1%) of g_{sw} at C_a of 400 µmol mol^{-1}. All A-C_i curves were fit using the 'bilinear' approach (which treats the FvCB model as a change-point model during curve fitting similar to Gu et al., 2010) of the {plantecophys} package in R (Duursma, 2015). For species that had temperature response curve measured, we fit the modified Arrhenius model to the maximum Rubisco carboxylation (V_{cmax}) and maximum electron transport (J_{max}) rates.

Accounting for cuticle conductance causes a decrease in the calculated value of C_i, such that current calculations methods are systematically overestimating C_i (Fig. 4a, c, e). These differences are least pronounced for A-C_i curve data (Fig. 4c), and most pronounced for temperature response data. In some instances, the C_i calculations breakdown when g_{cw} approaches the value of g_{sw}. Accounting for g_{cw} alters the shape of the A-C_i response, and increases fitted values for V_{cmax} and J_{max}, although differences appear negligible until g_{cw} is ~1% of g_{sw} (Fig. 5). In light of the interpretations of Parkhurst (1994), we modelled the impact of combined CO_2 gradients and cuticle conductance on the perceived A/C_i response.

Modeling g_{ias} and W_i effects on gas exchange parameters

Considering the Eq. describing the surface to intercellular CO_2 concentration gradient:

$$A_{net} = g_{sc}(C_s - C_i) \qquad \text{Eq. 24}$$

where g_{sc} is stomatal conductance to CO_2, C_s is the CO_2 concentration at the leaf surface, and C_i is intercellular airspace CO_2 concentration. Eq. 24 can misrepresent the process, which according to Parkhurst (1994) would be:

$$A_{net} = g_{sc}(C_s - C_{i,es}) = \quad g_{ias}(C_{i,es} - C_{ias}) \qquad \text{Eq. 25}$$

where $C_{i,es}$ is the CO_2 concentration at the site of evaporating surfaces, g_{ias} is the conductance of CO_2 from the evaporative surfaces to the intercellular airspace, and C_{ias} is the concentration of CO_2 in the intercellular airspace. Note that under the Parkhurst (1994) definition, C_{ias} could represent a point anywhere in the intercellular airspace, while $C_{i,es}$ is assumed to be closer to the substomatal cavity than C_{ias}. If the evaporating surface is at the mesophyll cell surface, then Eq. 25 would have to account for this reversed order and be re-written as:

$$A_{net} = g_s(C_s - C_{ias}) = \quad g_{ias}(C_{ias} - C_{es}) \qquad \text{Eq. 26}$$

Furthermore, g_s needs to be corrected for cuticular conductance. Therefore, we can describe the conductance of CO_2 and water from the leaf surface to the intercellular airspace ($g_{s,ias}$) according to:

$$g_{s,ias} = \frac{1}{\frac{1}{g_s - g_c} + \frac{1}{g_{ias}}} \qquad \text{Eq. 27}$$

We can further include mesophyll conductance, g_m, to calculate total conductance of CO_2 and water from the leaf surface to the chloroplast (g_t):

$$g_t = \frac{1}{\frac{1}{g_s - g_c} + \frac{1}{g_{ias}} + \frac{1}{g_m}} \qquad \text{Eq. 28}$$

We can then model the implications of g_c and g_{ias} on C_i by varying their values. We linked Eq. 28 to a leaf-level model of photosynthesis:

$$A_{net} = V_{cmax}\frac{C_c - \Gamma^*}{C_c + K_c\left(1 + \frac{O_c}{K_o}\right)} - R \qquad \text{Eq. 29}$$

$$A_{net} = J\frac{C_c - \Gamma^*}{4C_c - 8\Gamma^*} - R \qquad \text{Eq. 30}$$

$$(J - 0.5\alpha I)(J - J_{max}) = 0 \qquad \text{Eq. 31}$$

where V_{cmax} is maximum rate of Rubisco carboxylation, O_c is the oxygen concentration in the chloroplast (210 mmol mol^{-1}), K_c is the Michaelis-Menten constant for Rubisco carboxylation, K_o is the Michaelis-Menten constant for Rubisco oxygenation, J_{max} is the maximum rate of electron transport, J is the rate of electron transport, α is the proportion of irradiance (I) absorbed by the leaf, R is respiration, and Γ* is the photorespiratory CO_2 compensation point. All values (except for V_{cmax} and J_{max}) were obtained from Bernacchi *et al*. (2001).

We assumed a V_{cmax} and J_{max} of 100 and 200, respectively, and modelled under light saturating conditions such that J = J_{max}. We modelled from a C_s of 50 to 2000 in 50 ppm intervals. For calculating E_s (to represent the 'measured' transpiration from a gas exchange cuvette) we used the following equation:

$$E_s = g_{sw}\frac{W_i - W_s}{P} \qquad \text{Eq. 32}$$

where E_s is stomatal transpiration, g_{sw} is stomatal conductance (ranging from 0.03 to 2.00 mol m^{-2} s^{-1}), W_i is the water concentration inside the leaf (assumed to be 100% saturation vapor pressure for this initial calculation, which was calculated according to Cernusak et al., 2018), W_s is the water vapor concentration at the leaf surface (assumed to be 50% saturation vapor pressure), and P is atmospheric pressure (assumed to be 100 kPa). We assumed leaf temperature was equal to air temperature of 298 K. Once E_s was calculated, we then altered our assumptions about W_i, changing it to 99% and 90% of saturation vapor pressure. Then for each different W_i scenario, we set g_{cw} to either 0 or 0.01, and g_{ias} to either 1.00 (Mott, 1988) or infinity. The C_i obtained when W_i = 100% saturation vapor pressure, g_{cw} = 0 and g_{ias} = infinity was used as the reference C_i. A_{net} was then modelled to obtain A/C_i responses (using both reference C_i

and the C_i obtained from each combination of W_i, g_{cw} and g_{ias}) which were then fit using {plantecophys} (Duursma, 2015) in R (R Core Team, 2018) to obtain V_{cmax} estimates.

Modeling the effects of g_{cw} and g_{ias} across a range of reference g_{sw} (i.e. the g_s 'measured' using a typical open-flow gas exchange system), we see that g_c has the greatest impact at low g_{sw}, with a negligible effect when $g_{cw}/g_{sw} < 1\%$ at a C_s of 400 ppm (Fig. 6). Finite g_{ias}, however, has a much larger impact on C_i, with its effect size increasing with g_{sw} (Fig. 6). This explains the Ci discrepancies observed in Table 1—larger discrepancy with low g_{sw} and smaller discrepancy with high g_{sw}. It is also possible that the discrepancies relate to C_{ias} being directly measured deeper in the intercellular airspace than the location of the evaporating surface such that the calculated C_i is $C_{i,es}$ and the differences are due to how the quantities are defined. In the case of leaves treated with ABA (e.g. Boyer 2015a,b; Tominaga & Kawamitsu, 2015a) or stress induced stomatal closure, g_{cw} could account for the majority of the impact, since the limit of the CO_2 gradient-related deviation in calculated and real C_i tends towards 0 as measured g_{sw} approaches 0. Looking at W_i, the impact of W_i assumptions is evident. A 1% reduction in W_i increases the C_i discrepancy by a few ppm (Fig. 6b), and a 10% reduction causes changes the discrepancy by over 20 ppm in some cases (Fig. 6c).

If we fit A/C_i curves in the presence of g_{cw} and finite g_{ias} and use the Moss & Rawlins (1963) assumptions, g_c has a relatively small impact on V_{cmax}, but is important in cases where $g_{cw} > 5\%$ of g_s, while g_{ias} causes a large depression in V_{cmax} across all g_{sw} used in simulations (Fig. 6g, h, i). As vapor pressure in the leaf is reduced from 100%, V_{cmax} estimates increase (Fig. 6g, h, i). Interestingly, with $g_{cw} > 0$, $g_{ias} < \infty$, internal vapor pressure < saturation vapor pressure and high g_{sw}, V_{cmax} estimations are close to the value used in the model (Fig. 6i). Based on these modeling analyses, the impact of finite g_{ias} may be of greater concern when estimating gas exchange parameters than g_c, and many of the large g_c values reported using C_i differentials between calculated and measured values may in fact be partially attributed to a finite g_{ias}. It is crucial to note, however, that cuticle water fluxes have been reported up to 65% of total water flux across a leaf (Šantrůček et al., 2004), and the relative influence of g_{ias} and g_{cw} depend

774 on the relative value of g_{sw}. Given our modeling results showing the different impact of
775 g_{cw} and g_{ias} on gas exchange data, it may be possible to construct a model capable of
776 estimating g_{cw} and g_{ias} from a data set. This would allow proper attribution of C_i
777 differentials to g_{cw} versus g_{ias}.
778
779 Given the impact when all three assumptions test above are violated, it is possible that
780 many (or even most) estimates of apparent V_{cmax} in the literature may still be 'correct' for
781 the wrong reasons. However, we would like to note important assumptions made in our
782 modeling: 1) resistances within the leaf are additive (which may not hold; Parkhurst,
783 1984), 2) Fickian (rather than Knudsen, which may occur; Dacey, 1987) diffusion
784 governs gas diffusion from outside to inside the leaf, 3) the leaf is treated one-
785 dimensionally rather than three-dimensionally (which will affect calculations: Parkhurst,
786 1977; Earles et al., 2018), 4) the air pressure differential from outside to inside the leaf
787 is 0 (evidence suggested this may not be correct, at least in the extreme case of lotus,
788 *Nelumbo*; Leuning, 1983; Dacey, 1987).
789
790
791 *Solving the failed assumption*
792 *When does it (not) work?*
793 Cuticular conductance has largely been assumed negligible and is often ignored in gas
794 exchange measurements, while CO_2 gradients are largely ignored - however this may
795 be due to partitioning g_{ias} into g_m (Evans et al. 1994), reducing the need to consider g_{ias}
796 when C_i is taken as $C_{i,es}$. To date, many of the Moss and Rawlins (1963) assumptions
797 have been shown to be incorrect in at least some cases (e.g. Hygen, 1951, 1953;
798 Slavik, 1958; Jarvis & Slatyer, 1970; Leuning, 1983; Parkhurst, 1984; Ward & Bunce,
799 1986; Dacey, 1987; Egorov & Karpushkin, 1988; Long et al., 1989; Karpushkin, 1994;
800 Boyer et al., 1997; Meyer and Genty, 1998; Šantrůček et al., 2004; Canny & Huang,
801 2006; Boyer 2015a; Boyer, 2015b; Tominaga and Kawamitsu, 2015a; Cernusak et al.,
802 2018; Tominaga et al., 2018, Cernusak et al. 2019). We summarize the assumptions
803 and their expected impact on C_i calculations in Fig. 8. However, it is important to note

804 that the assumptions have allowed major breakthroughs in our understanding of plant
805 physiology.
806
807 Our analysis of the effects of g_{cw} on gas exchange measurements suggests that C_i is
808 relatively unaffected when g_{cw} is less than 1% of g_{sw} across a range of irradiance, [CO_2],
809 and temperature, and has a relatively minor effect on fitted values of V_{cmax} and J_{max}.
810 Given that most values of g_{cw} measured to date are relatively low, and assuming g_{cw}
811 was measured correctly, it is likely below the 1% threshold in unstressed plants,
812 especially crops (Table 2; Schuster *et al.*, 2017), this would explain why the Moss and
813 Rawlins (1963) assumption that $g_{cw} = 0$ has been successful in advancing our
814 understanding of photosynthesis over the past six decades. In regard to g_m, accounting
815 for g_{cw} increases the value of g_m, however such effects are small across irradiance and
816 [CO_2] when g_{cw} is at or below 1% g_{sw} but become particularly important for the
817 temperature response of mesophyll conductance. When g_{cw} exceeds 1% of g_{sw}, the
818 calculations for mesophyll conductance broke down for the modeling, giving extremely
819 high and/or negative values for g_m, which is related to $C_{i,cuticle}$ dropping close to or below
820 C_c. Pons et al. (2009) recommended accounting for g_{cw} in g_m measurements, and our
821 modeling suggests that this is critical when looking at the temperature response of g_m,
822 and in cases where g_{cw} is very high relative to g_{sw}. We may thus expect significant
823 errors in gas exchange calculations when g_{sw} is low (i.e. low light, drought, and high
824 VPD conditions), and/or when g_{cw} is high (i.e. high temperature, well-watered plants).
825 Furthermore, considering chlorophyll fluorescence-based estimates of g_m (i.e. Harley et
826 al., 1992), sensitivity of g_m should be similar to the isotopic method as it is calculated via
827 Eq. 23, with the added caveat that C_c becomes sensitive to the estimate of the
828 photorespiratory CO_2 compensation point (Γ*). Since Γ* can be estimated from gas
829 exchange or Rubisco kinetics, the sensitivity of calculated g_m to g_{cw} via the variable J
830 method will depend on how Γ* is measured. In this regard, interpreting data from
831 drought and temperature stress experiments should proceed with caution if g_{cw} is
832 ignored.
833

834 CO_2 gradients within leaves have ontological consequences for gas exchange
835 measurements, in particular, the meaning of C_i (Parkhurst, 1994). If typical C_i estimates
836 are taken to be $C_{i,es}$ measurements, then the implications of a finite g_{ias} on data derived
837 from the C_i estimates are minimal, since g_{ias} is often subsumed into g_m (Evans et al.,
838 1994). If $C_{i,es}$ occurs at the surface of the mesophyll cells, then g_{ias} will have no impact
839 on C_i estimates since the g_{sw} calculation occurs at the location of the evaporating
840 surface (Parkhurst, 1994). However, if the $C_{i,es}$ is located closer to the stomata than C_{ias}
841 (i.e. if the evaporating surface is not the mesophyll cell surface), C_{ias} would then be
842 located closer to the mesophyll cells than $C_{i,es}$. Our modeling of finite g_{ias} represents this
843 case and demonstrates that the implications of g_{ias} on data derived from such C_i
844 estimates can be quite large, causing C_i estimates to differ by >10 μmol mol^{-1}, and g_{sw}
845 to be reduced by more than 50% (Fig. 6). To reiterate, subsuming g_{ias} into g_m eliminates
846 the consequences of g_{ias} for 'C_i' estimates under conditions where C_{ias} lies closer to the
847 mesophyll cells than $C_{i,es}$. If $C_{i,es}$ is at the mesophyll cell surface, then g_{ias} is already
848 accounted for in g_{sw} calculations. As long as it is recognized that C_i estimates represent
849 $C_{i,es}$ (Parkhurst, 1994) and that all derived parameters are apparent parameters on a
850 $C_{i,es}$-basis, g_{ias} poses minimal issues to the interpretation of C_i data. This becomes an
851 issue however, in cases where the location of the evaporating surface differs between
852 species or treatment groups (e.g. control versus drought stress). The same would be
853 true for parameters derived from C_{ias} estimates if the rest of g_m were ignored. Note that
854 this underscores the importance of knowing the location of the C_i calculation. However,
855 it appears that g_{ias} has minimal consequences for g_m relative to g_{cw} at low values of g_{sw}
856 (Fig. 7), with g_{ias} shifting the g_{sw} value at which g_{cw} has the greatest impact on g_m.
857 Reducing W_i tends to reduce the impact of g_{cw} and g_{ias} on g_m (Fig. 7). We also
858 calculated the theoretical maximum values for g_{ias} based on leaf thicknesses from
859 Onoda et al. (2011) to estimate diffusion distances, along with biophysical equations to
860 calculate conductance (Massman, 1998; Campbell & Norman, 1998) (see
861 Supplementary Methods for more information on the calculations). We calculated that
862 the median maximum theoretical values of g_{ias} for an amphistomatous and
863 hypostomatous leaf is 24 and 3 mol m^{-2} s^{-1}, respectively (Fig. 1c).
864

So far, the above cases refer to conditions where W_i is at saturation vapor pressure. in cases where W_i is not at saturation vapor pressure inside the leaf (e.g. Cernusak et al., 2018), the consequences vary with the degree to which the assumption is violated. C_i, g_{sw}, and V_{cmax} are relatively unaffected when W_i is at 99% saturation (data not shown; note that xylem water potential is ~ -200 kPa (Nonami & Boyer, 1987), which would have a W_i value of ~99.85% saturation vapor pressure), however these parameters become both over- and under-estimated when W_i reaches 90% saturation depending on which assumptions are violated (Fig. 6). Thus, it appears that very small violations of this assumption will have minimal effects on gas exchange parameters. But caution must be exercised in cases where this assumption is likely to be violated, such as high vapor pressure deficit conditions, drought stress, and at high temperatures, as parameters will be overestimated. We note that there could be cases of multiple assumption violations leading to 'correct' parameters for the wrong reasons (i.e. Figs. 6h,i), although even in these cases other parameters are still different.

Based on our modeling, we predict that under conditions where g_{sw} is low (well-watered, low light, high [CO_2], low vapor pressure deficit, high leaf water potential), cuticular water loss will be sufficient to cause calculations to overestimate C_i (Fig. 2). Under conditions where W_i is less than expected (drought, high vapor pressure deficit, high temperature), calculated C_i values will be lower than the actual C_i (inside the mesophyll cells in Fig. 2b). As g_{ias} becomes increasingly finite, the C_i estimates will change in meaning from C_{ias} to $C_{i,es}$, barring violations in the other assumptions. Lastly, under conditions where g_{sw} is high, g_{cw} is minimal, g_{ias} is very high, and the assumptions of Moss and Rawlins (1963) hold, then calculated C_i and measured C_i should agree. However, in this last case, the agreement results from C_i meaning C_{ias}, which means that the assumptions behind g_m measurements need to be adjusted accordingly.

Cuticular water loss could be a significant source of water flux across the leaf and has the potential to undermine the assumptions upon which gas exchange calculations are based. We urge caution when performing and interpreting measurements of g_m due to the potential impact of g_{cw} on g_m calculations. More research is needed to assess the

magnitude of cuticular water loss across species and climates, however our data suggest that g_{cw} must exceed 1% of g_{sw} to have a substantial impact on photosynthetic gas exchange. Current information on the g_{cw} suggests that it may exceed that 1% threshold on average, depending on the measurement methodology. Combining the information from Riederer and Schreiber (2001) and Schuster et al. (2017), median g_c based on all methods was 1.84 mmol m^{-2} s^{-1} (IQR: 0.45 – 4.67 mmol m^{-2} s^{-1}, mean: 2.73 mmol m^{-2} s^{-1}), while median g_c based on permeance was 0.32 mmol m^{-2} s^{-1} (IQR: 0.11 – 0.90 mmol m^{-2} s^{-1}, mean: 0.85 mmol m^{-2} s^{-1}) and 3.31 mmol m^{-2} s^{-1} (IQR: 1.58 – 5.91 mmol m^{-2} s^{-1}, mean: 3.82 mmol m^{-2} s^{-1}) based on minimum conductance methods (Fig. 1a). Meanwhile, g_{sw} from the global datasets of Lin et al. (2015) and Smith and Dukes (2017) was 104 mmol m^{-2} s^{-1} (IQR: 52 – 226 mmol m^{-2} s^{-1}, mean: 185 mmol m^{-2} s^{-1}), suggesting that based on median values, cuticle conductance could range between 0.31 and 3.2 % of g_{sw} (Fig. 1). Schuster et al. (2017) note that minimum conductance methods can be biased towards high values if stomata are not completely closed, which may explain the 10-fold difference in median permeance between the methods. Another possible explanation for this discrepancy could be related to stretching of the cuticle at high Ψ, which enhances g_{cw} (Boyer et al., 1997) and would be the case for many minimum conductance measurements but not for permeance methods, where isolated cuticle could shrink (Boyer, 2015). We also note the large discrepancy in sample sizes for estimates of g_{sw} (> 22,000 observations) and g_{cw} (404 observations and only 148 for permeance-based methods). The development of a rapid method for assessing g_{cw} would help in circumventing broken assumptions when g_{cw}/g_{sw} is high.

The source of cuticular water loss is (un)clear: some evidence suggests that the bulk of cuticular water loss occurs across the guard cell cuticles rather than the epidermal surface (Šantrůček et al., 2004). Such heterogeneity in cuticular conductance across a leaf would need to be accounted for to obtain accurate C_i estimates, especially if epidermal and guard cell cuticular water loss show differential responses to leaf turgor. This would only matter if the change in permeability with turgor of the guard cells was greater than the change in permeability with turgor in other cells on the leaf surface. However, much of the work measuring cuticle conductance focuses on either isolated

cuticle from astomatous leaf surface or a gravimetric determination of cuticle conductance, with assumptions on stomatal opening and closure.

However, we note that part of the apparent effect of cuticle conductance in some studies may be due to CO_2 gradients (finite g_{ias}) within leaves. In fact, both processes can result in similar effects at low g_{sw} (Parkhurst, 1994; Fig. 6a), and each process could explain the evidence supporting the other process making partitioning difficult. Therefore, partitioning the impacts of g_{cw} and g_{ias} on C_i estimates should be a research priority.

Recommendations

We recommend the following:

1. Whenever possible, measure water potential (ideally $\Psi_{m,apo}$) to estimate W_i inside the leaf.
2. If measurements are not possible, choose suitable values of Ψ from the literature and calculate W_i.
3. Be clear as to the definition of C_i: is it $C_{i,es}$, C_{ias} or some other value? This will ensure that gas exchange parameters can be properly compared without confounding different aspects of leaf physiology.

In terms of understanding g_m, it is apparent that splitting g_m into its component parts (e.g. g_{ias}, g_{liq}) is necessary to understand how internal conductances respond to the environment. Given the likelihood of the variable location of C_i during most g_m measurements, many of the g_m measurements may not be directly comparable as they would be comparing different resistance pathways. Given that recent data assessing W_i inside leaves focused on xerophytic leaves (Cernusak et al., 2018), more data are needed to understand how W_i varies across environmental conditions in more mesophytic species, and especially angiosperms.

As a community, we have made significant advances within the Moss & Rawlins (1963) paradigm. Technological advances are now making it possible and crucial to move

beyond the Moss & Rawlins paradigm to further our understanding of photosynthesis and gaseous diffusion in leaves by addressing each of the assumptions (Fig. 8).

Code and Data

All code is available as supplementary files ("Modeling.rmd", "Reanalysis of gm data.rmd", "Literature gc-gs-gias calculations.rmd"), as are input data ("popexample.csv", "CO2response.csv", "temp data.csv", "gmlight.csv", "cuticle conductance temp response.csv", "cuticle_bins.csv", "WP.csv", "Diffusion bins Onoda data.csv"). Modeling code automatically generates .csv files for the modeling analysis.

Acknowledgements

We would like to thank Dr. Patrick J. Hudson for comments on an early draft of the manuscript and Dr. John S. Boyer for comments on a late draft. We would like to thank Yusuke Onoda for providing data on leaf thicknesses from Onoda et al. (2011) and Jordi Martínez-Vilalta for providing water potential data from Martínez-Vilalta et al. (2014). This work was also supported by funding to DTH through the NSF EPSCoR Program under Award # IIA-1301346 and through NSF IOS 1658951 at the University of New Mexico. Any opinions, findings, and conclusions or recommendations expressed in this material are those of the authors and do not necessarily reflect the views of the National Science Foundation. J.T. is supported by Research Fellowships for Young Scientists from the Japan Society for the Promotion of Science (JSPS).

Author Contributions

All authors contributed to the design of the study. JRS performed the modeling. JRS wrote the manuscript with input from all authors.

References

Bargel H, Kock K, Cerman Z, Neinhuis C. 2006. Evans review no. 3: structure-function relationships of the plant cuticle and cuticular waxes – a smart material? *Functional Plant Biology* 33, 893-910.

Boyer JS. 2015*a*. Turgor and the transport of CO_2 and water across the cuticle (epidermis) of leaves. *Journal of Experimental Botany* **66**, 2625–2633.

Boyer JS. 2015*b*. Impact of cuticle on calculations of the CO2 concentration inside leaves. *Planta* **242**, 1405–1412.

Boyer JS, Kawamitsu Y. 2011. Photosynthesis gas exchange system with internal CO_2 directly measured. *Environmental and Biological Control* **49**, 193-207.

Boyer JS, Wong SC, Farquhar GD. 1997. CO_2 and water vapor exchange across leaf cuticle (epidermis) at various water potentials. *Plant Physiology* **114**, 185–191.

Brown HT, Escombe F. 1900. Static diffusion of gases and liquids in relation to the assimilation of carbon and translocation in plants. *Philosophical Transactions of the Royal Society B* **193**: 185-193.

Buckley TN, Farquhar GD, Mott KA. 1997. Qualitative effects of patchy stomatal conductance distribution features on gas-exchange calculations. *Plant, Cell & Environment* **20**: 867-880.

Buckley TN, John GP, Scoffoni C, Sack L. 2017. The sites of evaporation within leaves. *Plant Physiology* 173:1763-1782.

Buckley TN, Sack L. 2019. The humidity inside leaves and why you should care: implications of unsaturation of leaf intercellular airspaces. *American Journal of Botany* 106(5):1-4.

Campbell GS, Norman JM. 1998. An introduction to environmental biophysics. Springer-Verlag, New York.

Canny MJ, Huang CX. 2006. Leaf water content and palisade cell size. *New Phytologist* **170**: 75-85.

Cernusak LA, Goldsmith GR, Arend M, Siegwolf, RTW. 2019. Effect of vapor pressure deficit on gas exchange in wild-type and abscisic acid-insensitive plants. *Plant Physiology* online early DOI:10.1104/pp.19.00436

Cernusak LA, Ubierna N, Jenkins MW, Garrity SR, Rahn T, Powers HH, Hanson DT, Sevanto S, Wong SC, McDowell NG, Farquhar GD. 2018. Unsaturation of vapour pressure inside leaves of two conifer species. *Scientific Reports* **8**: 7667.

Cheeseman JM, Clough BF, Carter DR, Lovelock CE, Eong OJ, Sim RG. 1991. The analysis of photosynthetic performance in leaves under field conditions: a case study using *Bruguiera* mangroves. *Photosynthesis Research*, **29**, 11-22.

Dacey JWH. 1981. Pressurized ventilation in the yellow waterlily. *Ecology* **62**: 1137-1147.

Dacey JWH. 1987. Knudsen-transitional flow and gas pressurization in leaves of *Nelumbo*. *Plant Physiology* **85**: 199-203.

Douthe C, Dreyer E, Epron D, Warren CR. 2011. Mesophyll conductance to CO_2, assessed from online TDL-AS records of $^{13}CO_2$ discrimination, displays small but significant short-term responses to CO_2 and irradiance in *Eucalyptus* seedlings. *Journal of Experimental Botany* **62**, 5335–5346.

Downton WJS, Loveys BR, Grant WJR. 1988. Non-uniform stomatal closure induced by water stress causes putative non-stomatal inhibition of photosynthesis. *New Phytologist* **110**: 503-509.

Earles JM, Théroux-Rancourt G, Roddy AB, Gilbert ME, McElrone AJ, Brodersen C. 2018. Beyond porosity: 3D leaf intercellular airspace traits that impact mesophyll conductance. *Plant Physiology* **178**, 148-162.

Egorov VP, Karpushkin LT. 1988. Determination of air humidity over evaporating surface inside a leaf by a compensation method. *Photosynthetica* **22**: 394-404.

Evans J. 1995. Carbon fixation profiles do reflect light absorption profiles in leaves. *Australian Journal of Plant Physiology* **22**, 865-873.

Evans JR, Caemmerer SV, Setchell BA, Hudson GS. 1994. The relationship between CO_2 transfer conductance. *Australian Journal of Plant Physiology* **21**: 475-495.

Evans JR, Loreto F. 2000. Acquisition and diffusion of CO_2 in higher plant leaves. In: Leegood, R. C., Sharkey, T. D., von Caemmerer, S. eds. Photosynthesis: Physiology and Metabolism, Kluwer Academic Publishers, Netherlands, 321–351.

Farquhar GD, von Caemmerer S, Berry JA. 1980. A biochemical model of photosynthetic CO_2 assimilation in leaves of C_3 species. *Planta* **149**, 78–90.

Farquhar GD, Cernusak LA. 2012. Ternary effects on the gas exchange of isotopologues of carbon dioxide. *Plant, Cell & Environment* **35**, 1221–1231.

Farquhar G, O'Leary M, Berry J. 1982. On the relationship between carbon isotope discrimination and the intercellular carbon dioxide concentration in leaves. *Australian Journal of Plant Physiology* **9**, 121.

Farquhar GD, Raschke K. 1978. On the resistance to transpiration of sites of evaporation within leaf. *Plant Physiology* **61**: 1000-1005.

Flexas J, Bota J, Escalona JM, Sampol B, Medrano H. 2002. Effects of drought on photosynthesis in grapevines under field conditions: an evaluation of stomatal and mesophyll limitations. *Functional Plant Biology* **29**, 461.

Gaastra P. 1959. Photosynthesis of crop plants as influenced by light, carbon dioxide, temperature, and stomatal diffusion resistance. *Mededelingen van de Landbouwhogeschool te Wageningen, Nederland* **59**: 1-68.

Gimenez C, Mitchell VJ, Lawlor DW. 1992. Regulation of photosynthetic rate of two sunflower hybrids under water stress. *Plant Physiology* **98**: 516-514.

Gunasekera D, Berkowitz GA. 1992. Heterogenous stomatal closure in response to leaf water deficits is not a universal phenomenon. *Plant Physiology* **98**: 660-665.

Hall AE. 1982. Mathematical models of plant water loss and plant water relations. In: Lange OL, Nobel PS, Osmond CB, Ziegler H, eds. Physiological plant ecology II. Berlin, Heidelberg: Springer Berlin Heidelberg, 231–261.

Hoad SP, Grace J, Jeffree CE. 1996. A leaf disc method for measuring cuticular conductance. *Journal of Experimental Botany* **47**: 431-437.

Hygen G. 1951. Studies in plant transpiration I. *Physiologia Plantarum* **4**: 57-183.

Hygen G. 1953. Studies in plant transpiration II. *Physiologia Plantarum* **6**: 106-133.

Jarvis PG, Slatyer RO. 1970. The role of the mesophyll cell wall in leaf transpiration. *Planta* **80**: 303-322.

Jones HG, Higgs KH. 1980. Resistance to water loss from mesophyll cell surface in plant leaves. *Journal of Experimental Botany* **31**: 545-553.

Karpushkin LT. 1994. A compensation gasometric method for estimating the kinetic parameters of H_2O and CO_2 exchange in plant leaves. *Russian Journal of Plant Physiology* **41**: 410-413.

Kerstiens G. 1996a. Cuticular water permeability and its physiological significance. *Journal of Experimental Botany* **47**: 1813-1832.

Kerstiens G. 1996b. Diffusion of water vapour and gases across cuticles and through stomatal pores presumed closed. In: **Kerstiens G**, ed. *Plant cuticles: and integrated functional approach* Oxford: Bios, 121-133.

Kirschbaum MUF, Pearcy RW. 1988. Gas exchange analysis of the relative importance of stomatal and biochemical factors in photosynthetic induction in *Alocasia macrorrhiza*. *Plant Physiology* **86**: 782-785.

Laisk A, Ojs V, Kull K. 1980. Statistical distribution of stomatal apertures of Vicia faba and Hordeum vulgare and the Spannungsphase of stomatal opening. *Journal of Experimental Botany* **31**, 49-58.

Lauer MJ, Boyer JS. 1992. Internal CO_2 measured directly in leaves: Abscisic acid and low leaf water potential cause opposing effects. *Plant Physiology* **98**, 1310-1316.

Lawlor DW. 2002. Limitation to Photosynthesis in Water-stressed Leaves: Stomata vs. Metabolism and the Role of ATP. *Annals of Botany* **89**, 871–885.

Lawson T, James W, Weyers J. 1998. A surrogate measure of stomatal aperture. *Journal of Experimental Botany*, **49**, 1397-1403.

Ledford H. 2017. Overlooked water loss in plants could throw off climate models. *Nature* **546**, 585–586.

Leuning R. 1983. Transport of gases into leaves. *Plant, Cell & Environment* **6**: 181-194.

Lin Y-S, Medlyn BE, Duursma RA, Prentice IC, Wang H, et al. 2015. Optimal stomatal behaviour around the world. *Nature Climate Change* **5**, 459–464.

Long SP, Farage PK, Bolhár-Nordenkampf HR, Rohrhofer U. 1989. Separating the contribution of the upper and lower mesophyll to photosynthesis in *Zea mays* L. leaves. *Planta* **177**, 207–216.

Li-Cor. 2019. Using the LI-6800 portable photosynthesis system. *Li-Cor Biosciences*, Lincoln, NB.

McAusland L, Davey PA, Kanwal N, Baker NR, Lawson T. 2013. A novel system for spatial and temporal imaging of intrinsic plant water use efficiency. *Journal of experimental botany* **64**, 4993-5007.

Mansfield LA, Hetherington AM, Atkinson CJ. 1990. Some current aspects of stomatal physiology. *Annual Review of Plant Physiology and Plant Molecular Biology* **41**, 55–75.

Martínez-Vilalta J, Poyatos R, Aquadé D, Retana J, Mencuccini M. 2014. A new look at water transport regulation in plants. *New Phytologist* **204**, 105-115.

Massman WJ. 1998. A review of the molecular diffusivities of H_2O, CO_2, CH_4, CO, O_3, SO_2, NH_3, N_2O, NO, and NO_2 in air, O_2 and N_2 near STP. *Atmospheric Environment* **32**, 1111-1127.

Meyer S, Genty B. 1998. Mapping intercellular CO_2 mole fraction (C_i) in *Rosa rubiginosa* leaves fed with abscisic acid by using chlorophyll fluorescence imaging. Significance of C_i estimated from leaf gas exchange. *Plant Physiology* **116**, 947–957.

Mott KA. 1988. Do stomata respond to CO_2 concentrations other than intercellular? *Plant Physiology* **86**, 200-203.

Mott KA, Buckley TN. 2000. Patchy stomatal conductance: emergent collective behavious of stomata. *Trends in Plant Science* **5**: 258-262.

Nobel P. 1991. Physicochemical and environmental plant physiology. Academic Press San Diego.

Nonami H, Boyer JS. 1987. Origin of growth-induced water potential. *Plant Physiology* **83**, 596-601.

Nonami H, Schulze E-D, Ziegler H. 1991. Mechanisms of stomatal movement in response to air humidity, irradiance and xylem water potential. *Planta* **183**: 57-64.

Oleson KW, Lawrence DM, Bonan GB, Dreniak B, Huang M, Koven CD, Levis S, Li F, Riley WJ, Subin ZM, et al. 2013. Technical description of version 4.5 of the Community Land Model (CLM). Boulder, CO: National Center for Atmospheric Research.

Onoda Y, Westoby M, Adler PB, Choong AMF, Clissold FJ, Cornelissen JHC, Diaz S, Dominy NJ, Elgart A, Enrico L, et al. 2011. Global patterns of leaf mechanical properties. *Ecology Letters* **14**, 301-312.

Parkhurst DF. 1994. Diffusion of CO_2 and other gases inside leaves. *New Phytologist* **126**: 449-479.

Parkhurst DF. 1984. Mesophyll resistance to photosynthetic carbon dioxide uptakes in leaves: dependence on stomatal aperture. *Canadian Journal of Botany* **62**: 163-165.

Parkhurst DF. 1977. A three-dimensional model for CO_2 uptake by continuously distributed mesophyll in leaves. *Journal of Theoretical Biology* **67**: 471-488.

Parkhurst DF, Mott KA. 1990. Intercellular diffusion limits to CO_2 uptake in leaves. *Plant Physiology* **94**: 1024-1032.

Parkhurst DF, Wong S-C, Farquhar GD, Cowan IR. 1988. Gradients of intercellular CO_2 levels across the leaf mesophyll. *Plant Physiology* **86**: 1032-1037.

Pons TL, Flexas J, von Caemmerer S, Evans JR, Genty B, Ribas-Carbo M, Brugnoli E. 2009. Estimating mesophyll conductance to CO_2: methodology, potential errors, and recommendations. *Journal of Experimental Botany* **60**, 2217–2234.

Riederer M, Schreiber L. 2001. Protecting against water loss: analysis of the barrier properties of plant cuticles. *Journal of Experimental Botany* **52**, 2023–2032.

Šantrůček J, Šimáňová E, Karbulková J, Šimková M, Schreiber L. 2004. A new technique for measurement of water permeability of stomatous cuticular membranes isolated from *Hedera helix* leaves. *Journal of Experimental Botany* **55**: 1411-1422.

Scafaro AP, Von Caemmerer S, Evans JR, Atwell BJ. 2011. Temperature response of mesophyll conductance in cultivated and wild *Oryza* species with contrasting mesophyll cell wall thickness. *Plant, Cell & Environment* **34**, 1999–2008.

Schuster A-C, Burghardt M, Riederer M. 2017. The ecophysiology of leaf cuticular transpiration: are cuticular water permeabilities adapted to ecological conditions? *Journal of Experimental Botany* **68**, 5271–5279.

Sharkey TD, Seemann JR. 1989. Mild water stress effects on carbon-reduction-cycle intermediates, ribulose bisphosphate carboxylase activity, and spatial homogeneity of photosynthesis in intact leaves. *Plant Physiology* **89**: 1060-1065.

Sharkey TD, Imai K, Farquhar GD, Cowan IR. 1982. A direct confirmation of the standard method of estimating intercellular partial pressure of CO_2. *Plant Physiology* **69**, 657–659.

Slavik B. 1958 The influence of water deficit on transpiration. *Physiologia Plantarum* **11**: 524-535.

Smith NG, Dukes JS. 2017. LCE: leaf carbon exchange data set for tropical, temperate, and boreal species of North and Central America. *Ecology* **98**.

Steinberg SL. 1996. Mass and energy exchange between the atmosphere and leaf influence gas pressurization in aquatic plants. *New Phytologist* **134**: 587-599.

Stinziano JR, Morgan PB, Lynch DJ, Saathoff AJ, McDermitt DK, Hanson DT. 2017. The rapid A-C_i response: photosynthesis in the phenomic era. *Plant, Cell & Environment* **40**, 1256–1262.

Terashima I, Wong SC, Osmond CB, Farquhar GD. 1988. Characterization of non-uniform photosynthesis induced by abscisic acid in leaves having different mesophyll anatomies. *Plant and Cell Physiology* **29**, 385–394.

Terashima I. 1992. Anatomy of non-uniform leaf photosynthesis. *Photosynthesis research*, **31**, 195–212.

Tezara W, Mitchell VJ, Driscoll SD, Lawlor DW. 1999. Water stress inhibits plant photosynthesis by decreasing coupling factor and ATP. *Nature* **401**: 914-917

Tholen D, Zhu X-G. 2011. The mechanistic basis of internal conductance: a theoretical analysis of mesophyll cell photosynthesis and CO_2 diffusion. *Plant Physiology* **178**

Tominaga J, Kawamitsu Y. 2015*b*. Tracing Photosynthetic Response Curves with Internal CO_2 measured directly. *European Chemical Bulletin* **53**, 27–34.

Tominaga J, Kawamitsu Y. 2015*a*. Cuticle affects calculations of internal CO_2 in leaves closing their stomata. *Plant & Cell Physiology* **56**, 1900–1908.

Tominaga J, Shimada H, Kawamitsu Y. 2018. Direct measurement solves overestimation of intercellular CO_2 concentration in leaf gas-exchange measurements. *Journal of Experimental Botany* **69**, 1981-1991.

Van Gardingen PR, Jeffree CE, Grace J. 1989. Variation in stomatal aperture in leaves of *Avena latua* L observed by low-temperature scanning electron microscopy. *Plant Cell & Environment* **12**, 887-898.

Vogel JC. 1980. Fractionation of the carbon isotopes during photosynthesis. Fractionation of the carbon isotopes during photosynthesis. Berlin, Heidelberg: Springer Berlin Heidelberg, 5–29.

Vrábl D, Vasková M, Hronková M, Flexas J, Santrucek J. 2009. Mesophyll conductance to CO_2 transport estimated by two independent methods: effect of variable CO_2 concentration and abscisic acid. *Journal of Experimental Botany* **60**, 2315–2323.

Ward DA, Bunce JA. 1986. Novel evidence for a lack of water-vapor saturation within the intercellular airspace of turgid leaves of mesophytic species. *Journal of Experimental Botany* **37**: 504-516.

West JD, Peak D, Peterson JQ, Mott KA. 2005. Dynamics of stomatal patches for a single surface of *Xanthium strumarium* L. leaves observed with fluorescence and thermal images. *Plant, Cell & Environment* **28**, 633-641.

Weyers JDB, Lawson T. 1997. Heterogeneity in stomatal characteristics. *Advances in Botanical Research* **26**: 317-352.

Wingate L, Seibt U, Moncrieff JB, Jarvis PG, Lloyd J. 2007. Variations in 13C discrimination during CO_2 exchange by *Picea sitchensis* branches in the field. *Plant, Cell & Environment* **30**, 600–616.

Wise RR, Ortiz-Lopez A, Ort DR. 1992. Spatial distribution of photosynthesis during drought in field-grown and acclimated and nonacclimated growth chamber-grown cotton. *Plant Physiol*ogy **100**, 26-32.

Tables

Table 1. Reported C_i for direct tests of the Moss and Rawlins (1963) assumptions.

Species	Experiment	g_{sw} ($mmol\ m^{-2}\ s^{-1}$)	C_a ($\mu mol\ mol^{-1}$)	C_i differential[a]	Study
		mean / single / range			
Hypostomatous leaves					
Vitis vinifera (both sides)	control	178	350	3	Boyer *et al.* (1997)
	high CO_2	19	1100	126	
Vitis vinifera (astomatous side)[d]	control	4.4	350	291	
	high CO_2	4.2	1100	940	
Vitis vinifera[c] (astomatous side)[d]	high CO_2	0.73	10000	9436	Boyer (2015b)
Passiflora edulis (astomatous side)[d]	various T_{leaf}	0.21	400	267 – 432	Tominaga *et al.* (2018)
Amphistomatous leaves					
Xanthium strumarium[b]	various CO_2	not reported	88 – 619	3 – 9	Sharkey *et al.* (1982)
	various light		333 – 349	-10 – 0	
	dark		352	-19	
Gossypium hirsutum[b]	various VPD		330	-14 – 14	
Brassica chinensis[b]	various species	not reported	309 – 338	31	Parkhurst et al. (1988)
Eucalyptus pauciflora[b]				54	
Gossypium hirsutum[b]				24	
Phaseolus vulgaris[b]				29	
Spinacia oleracea[b]				34	
Helianthus annuus	very high CO_2	260-280	10000 – 50000	<150	Boyer & Kawamitsu (2011)
Helianthus annuus	control	205	400	30	Boyer (2015a)
	ABA	37		245	
Helianthus annuus	A/Ci curve	248 – 488	34 – 1556	-10 – 36	Tominaga & Kawamitsu (2015*b*)
	A/Ci curve ABA	18 – 86	31 – 1982	-10 – 451	
Helianthus annuus	A/Ci curve	264 – 307	24 – 320	-4 – 0	Tominaga *et al.* (2018)
Phaseolus vulgaris	A/Ci curve high SD	336 – 401	24 – 344	-1 – 4	
	A/Ci curve low SD	37 – 40	22 – 652	-6 – 166	

Data were retrieved from either texts or figures unless the raw data are available.

[a] C_i differential=Calculated C_i – measured C_i

[b] CO_2 concentrations are shown in μbar. 1 μbar is 1 $\mu mol\ mol^{-1}$ at standard pressure of 1013 bar.

[c]Ci was recalculated from Fig. 2 in Boyer (2015b), according to the model by von Caemmer & Farquhar (1981).

[d]For gas exchange measurements on astomatous side in hypostomatous leaves, g_{sw} indicates cuticle conductance (g_{cw}).

Table 2. Cuticular permeances from Riederer and Schreiber (2001) re-interpreted as cuticular conductance (g_{cw}) and transpiration (E_c).

Species	Temperature (K)	Permeance (m s^{-1} x 10^6)	g_{cw} (mmol m^{-2} s^{-1})	E_c (µmol m^{-2} s^{-1})	Source
Citrus aurantium	298	71.0	0.29	9.1	Baur, 1997
Ficus elastica	298	18.0	0.07	2.3	
Hedera helix	298	7.4	0.03	0.9	
Pyrus communis	298	670.0	2.76	85.6	
Stephanotis floribunda	298	330.0	1.36	42.2	
Citrus aurantium	298	120.0	0.49	15.3	Becker *et al*., 1986
Clivia miniata	298	11.0	0.05	1.4	
Ficus elastica	298	43.0	0.18	5.5	
Hedera helix	298	27.0	0.11	3.5	
Nerium oleander	298	33.0	0.14	4.2	
Pyrus communis	298	120.0	0.49	15.3	
Schefflera actinophylla	298	8.2	0.03	1.0	
Citrus aurantium	298	690.0	2.84	88.2	Geyer and Schonherr, 1990
Citrus aurantium	298	470.0	1.93	60.1	Haas and Schonherr, 1979
Anthurium brownii	303	11.5	0.05	1.9	Helbsing *et al*., 2001
Anthurium salviniae	303	6.8	0.03	1.1	
Aspasia principissa	303	4.6	0.02	0.8	
Caularthron bilamellatum	303	11.3	0.05	1.9	
Epidendrum nocturum	303	17.7	0.07	3.0	
Notylia pentachne	303	12.7	0.05	2.1	
Oncidium ampliatum	303	9.5	0.04	1.6	
Peperomia cordulata	303	46.1	0.19	7.8	
Philodendron radiatum	303	11.8	0.05	2.0	
Philodendron tripartitum	303	11.2	0.05	1.9	
Polystachya foliosa	303	60.7	0.25	10.2	

Sobralia fenzliana	303	26.6	0.11	4.5	
Sobralia suaveolens	303	16.9	0.07	2.8	
Trichopilia maculata	303	21.7	0.09	3.7	
Abies alba	293	1400.0	5.86	134.4	Lendzian *et al*., 1986
Citrus aurantium	293	450.0	1.88	43.2	
Camellia sinensis	298	57.8	0.24	7.4	Reiderer and Schreiber, 2001
Citrus aurantium	298	95.2	0.39	12.2	
Clivia miniata	298	4.8	0.02	0.6	
Clusia flava	298	20.2	0.08	2.6	
Clusia uvitana	298	48.7	0.20	6.2	
Clusia uvitana	298	137.0	0.56	17.5	
Corynocarpus laevigatus	298	49.7	0.20	6.4	
Cydonia oblongata	298	101.0	0.42	12.9	
Euonymus japonica	298	79.2	0.33	10.1	
Ficus elastica	298	14.6	0.06	1.9	
Ficus elastica	298	39.5	0.16	5.0	
Forsythia intermedia	298	86.2	0.35	11.0	
Garcinia spicata	298	63.8	0.26	8.2	
Hedera helix	298	21.7	0.09	2.8	
Monstera deliciosa	298	24.3	0.10	3.1	
Nerium oleander	298	40.0	0.16	5.1	
Philodendron ilsemanii	298	10.4	0.04	1.3	
Pyrus communis	298	63.4	0.26	8.1	
Pyrus communis	298	82.9	0.34	10.6	
Vanilla planifolia	298	3.6	0.01	0.5	
Allium cepa	298	190.0	0.78	24.3	Schonherr and Merida, 1981
Citrus aurantium	298	150.0	0.62	19.2	Schonherr and Schmidt, 1979
Citrus aurantium	298	280.0	1.15	35.8	
Camellia sinensis	298	46.8	0.19	6.0	Schreiber and Riederer, 1996b

Citrus aurantium	298	55.5	0.23	7.1
Citrus limon	298	204.0	0.84	26.1
Clivia miniata	298	68.1	0.28	8.7
Cydonia oblongata	298	273.0	1.12	34.9
Euonymus japonica	298	155.0	0.64	19.8
Ficus benjamina	298	56.4	0.23	7.2
Ficus elastica	298	40.7	0.17	5.2
Forsythia suspensa	298	168.0	0.69	21.5
Gingko biloba	298	226.0	0.93	28.9
Hedera helix	298	24.7	0.10	3.2
Juglans regia	298	199.0	0.82	25.4
Ligustrum vulgare	298	188.0	0.77	24.0
Liriodendron tulipifera	298	182.0	0.75	23.3
Maianthemum bifolium	298	481.0	1.98	61.5
Monstera deliciosa	298	18.6	0.08	2.4
Nerium oleander	298	226.0	0.93	28.9
Olea europaea	298	54.6	0.22	7.0
Philodendron selloum	298	28.6	0.12	3.7
Prunus laurocerasus	298	57.7	0.24	7.4
Vanilla planifolia	298	7.4	0.03	0.9

Figures

Figure 1 – Density plot of measured (a) cuticle (g_c), (b) stomatal (g_s) values, and (c) maximum theoretical intercellular airspace conductance (g_{ias}) values assuming diffusion through 12.5% of leaf thickness for amphistomatous leaves (Amphi) and 87.5% of leaf thickness for hypostomatous leaves (Hypo). (a) Data was compiled from Riederer and Schreiber (2001) and the supplementary information from Schuster et al. (2017). Black line indicates 1% of the median value from (b), while dashed lines indicate method-specific medians. (b) Data was compiled from Lin et al. (2015) and Smith and Dukes (2017). (c) Leaf thickness data used to calculate maximum g_{ias} from Onoda et al. (2011).

Figure 2 – Implications of intercellular water vapor concentration (W_i) as a percentage of saturation vapor pressure (VPD) for (a) conductance (g) calculations, and the effects of (b) water potential (Ψ) and (c) leaf to air vapor pressure deficit (VPD_{leaf}). a) When Ψ = 0 MPa, W_i = 100% e_s, and VPD = 0 kPa, then g represents stomatal conductance (g_s). When Ψ = 0 MPa, W_i = 100% e_s, and VPD > 0 kPa, then 1/g represents $1/g_s + 1/g_{ias}$ (intercellular airspace conductance). When Ψ < 0 MPa, W_i < 100% e_s, and VPD > 0 kPa, then 1/g represents $1/g_s + 1/g_{ias} + 1/g_{liq}$ where g_{liq} is liquid conductance into the cell. Potential locations of $C_{i,es}$ (CO_2 concentration at the evaporating surface) are indicated by black lines. b) As Ψ decreases, the location of calculated W_i recedes further into the leaf and into the cell. c) As VPD_{leaf} increases, the location of W_i recedes away from the substomatal cavity. C_c: chloroplastic CO_2 concentration, C_{ias}: CO_2 concentration of the intercellular airspace.

Figure 3 – Water use efficiency as a function of intercellular [CO_2] accounting for cuticular conductance ($C_{icuticle}$), and the relationship with the proportion of stomatal conductance attributed to cuticular conductance. iWUE: intrinsic water use efficiency.

Figure 4– The sensitivity of intercellular [CO_2] (C_i) (a, c, e) and mesophyll conductance (g_m) (b, d, f) to the proportion of stomatal conductance attributed to cuticle conductance.

(a) Data from Douthe et al. (2011); (b) Data from Vrabl et al. (2009); (c, d) Data from Scafaro et al. (2011) assuming (c) the highest temperature sensitivity of cuticular conductance or (d) the lowest temperature sensitivity of cuticular conductance from Riederer and Schreiber (2001). For unrestricted axes and C_i comparisons, see Figs. S1, S2; for g_m comparisons, see Figs. S3, S4, S5).

Figure 5 – a) Response of A_{net} to C_i under different g_{cw} scenarios. b) Response of g_{sw} to C_i under different g_{cw} scenarios. Solid lines indicate value of g_{cw} across curve. c) Response of V_{cmax} to J_{max} as a function of the proportion of g_{sw} attributed to g_{cw}. Re-interpreted A-C_i data extracted from Vrabl et al. (2009). A_{net}: net CO_2 assimilation; C_i: intercellular CO_2 concentration; g_{cw}: cuticle conductance to water; g_{sw}: stomatal conductance to water; J_{max}: maximum rate of electron transport to RuBP regeneration; Proportion: proportion of g_{sw} attributed to g_{cw} at a reference CO_2 of 400 µmol mol^{-1}; V_{cmax}: maximum rate of rubisco carboxylation capacity.

Figure 6 – Effects of CO_2 gradients (finite g_{ias}) and cuticle conductance (g_c) on calculated C_i (ΔC_i) (a, b, c), g_s (d, e, f), and ΔV_{cmax} (g, h, i), when intercellular water vapor concentration (W_i) is at 100% (a, d, g), 95% (b, e, h), and 90% (c, f, i) of saturation vapor pressure (e_s). g_{s_actual}: actual stomatal conductance given the assumptions; g_{s_ref}: reference g_s where g_c = 0, g_i mmol m^{-2} $s^{-1}{}_s$ = infinity, and W_i = 100% e_s; Ng_{ias}: no CO_2 gradient; Yg_{ias}: CO_2 gradient present, g_{ias} = 1000 mmol m^{-2} s^{-1}; Ng_c: g_c = 0 mmol m^{-2} s^{-1}; Yg_c: g_c = 10 mmol m^{-2} s^{-1}; ΔV_{cmax}: percent change in maximum rate of Rubisco carboxylation.

Figure 7 – Modelled impacts of intercellular [H_2O] (W_i), cuticle conductance (g_c), and intercellular airspace conductance (g_{ias}) on mesophyll conductance (g_m) expressed as a change in g_m (Δg_m (%)), across a range of reference g_s values (g_{s_ref}). W_i is either a) 100% saturation vapor presure (e_s), b) 95% e_s, or c) 90% e_s. Reference value for g_m is 0.48 mol m^{-2} s^{-1} at 1 atmosphere. For Δg_m < 10% in $Ng_{ias}Yg_c$, g_{s_ref} must exceed 0.187 mol m^{-2} s^{-1}, 0.168 mol m^{-2} s^{-1}, and 0.15 mol m^{-2} s^{-1} in a), b), and c), respectively. Ng_{ias}:

no CO_2 gradient; Yg_{ias}: CO_2 gradient present, g_{ias} = 1000 mmol m^{-2} s^{-1}; Ng_c: g_c = 0 mmol m^{-2} s^{-1}; Yg_c: g_c = 10 mmol m^{-2} s^{-1}.

Figure 8 – Relative effects of departures from each assumption on calculated C_i (C_{ic}) relative to actual C_i under constant A and constant measured conductance (g). **Assumption 1**: increasing g_{cw} causes C_{ic} to increase, leading to overestimation of C_i, with a stronger effect at lower g. **Assumption 2**: decreasing g_{ias} causes C_{ic} to increase, leading to overestimation of C_i, with a stronger effect at higher g. **Assumption 3**: decreasing W_i from 100% SVP causes C_{ic} to decrease, leading to underestimation of C_i, with a stronger effect at lower g. Decreasing leaf water potential ($\Psi_{m,apo}$) causes W_i to decrease, causing C_{ic} to decrease and underestimate C_i. **Assumption 4**: positively skewed stomatal apertures means that stomata are more closed than expected based on g, such that C_{ic} overestimates C_i. Likewise, negatively skewed stomatal apertures means that stomata are more open than expected based on g, such that C_{ic} underestimates C_i. This results from influences on g_{ias} – smaller than expected stomatal apertures means that the effective pathlength for diffusion is longer, decreasing g_{ias} relative to an "expected value", while larger than expected stomatal apertures means that the effective pathlength for diffusion is smaller, increasing g_{ias} relative to an "expected value". In the second case and under Assumption 2, the difference in g_{ias} would be a difference between a smaller and larger infinite value. **Assumption 5**: a pressurized leaf relative to air ($\Delta P_{leaf\text{-}to\text{-}air} > 0$) means that calculated W_i is higher than the expected e_s, causing C_{ic} to overestimate C_i, and a negatively pressurized leaf ($\Delta P_{leaf\text{-}to\text{-}air} > 0$) means that W_i is lower than the expected e_s, causing C_{ic} to underestimate C_i. Note that the pressure will also have implications for the diffusion dynamics, but we do not address them here. **Assumption 6**: when $D_{H2O}/D_{CO2} > 1.6$, g_{sc} is overestimated, causing C_{ic} to overestimate C_i, while $D_{H2O}/D_{CO2} < 1.6$ causes underestimation of g_{sc}, leading C_{ic} to underestimate C_i. Note that these effects are stronger under smaller values of g. **Assumption 7**: when considering gas exchange in 3-D, tortuosity of the pathway and homo/heterobaricity of the leaf (which could feed into tortuosity), and leaf thickness impact g_{ias}, with higher tortuosity, lower heterobaricity and thicker leaves, decreasing g_{ias}, causing C_{ic} to overestimate Ci. **Note**: tortuosity, heterobaricity, and leaf thickness will influence g_{ias}. Assumptions 3 and 5 feed into assumption 3, while assumptions 4 and 7 feed into assumption 2.

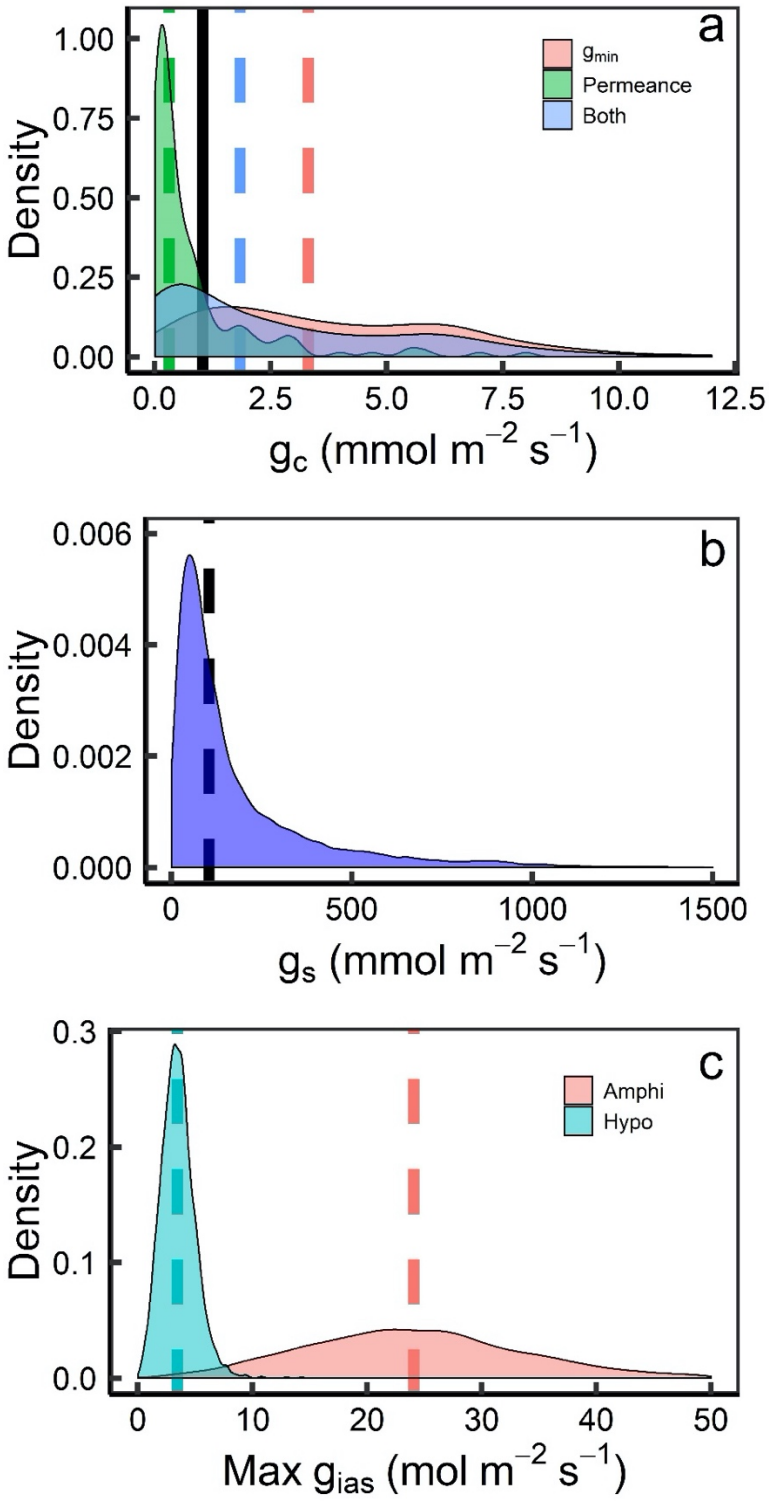

Figure 1

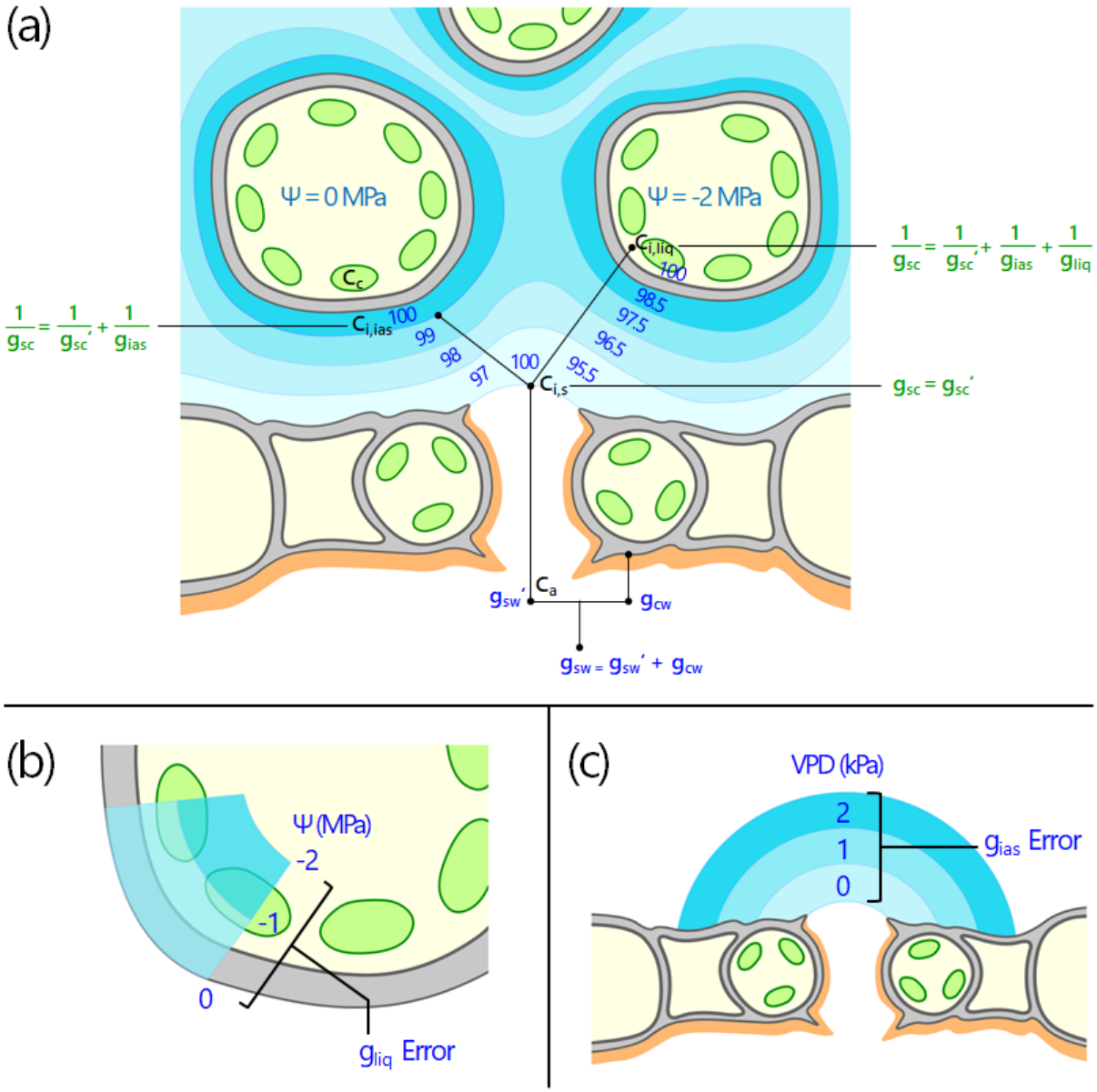

Figure 2

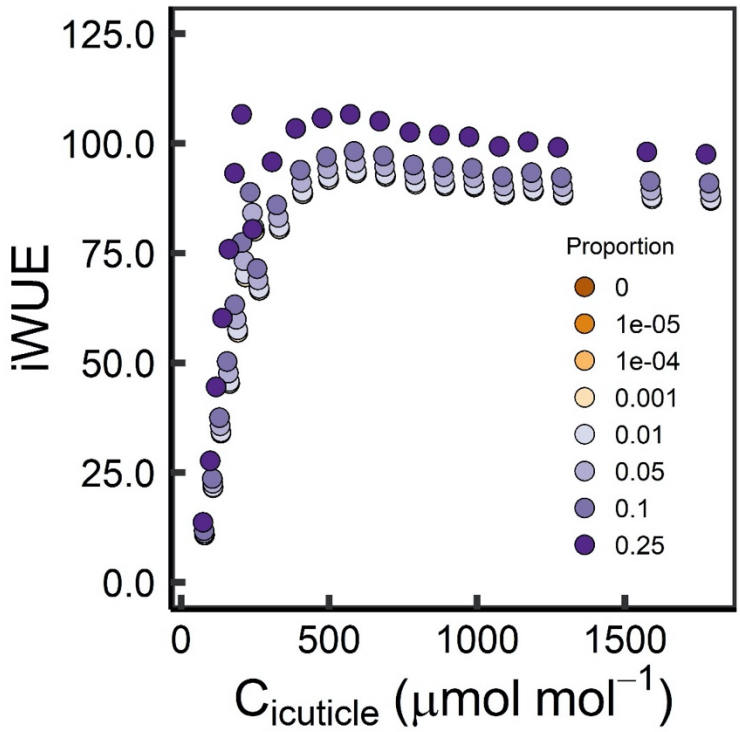

Figure 3

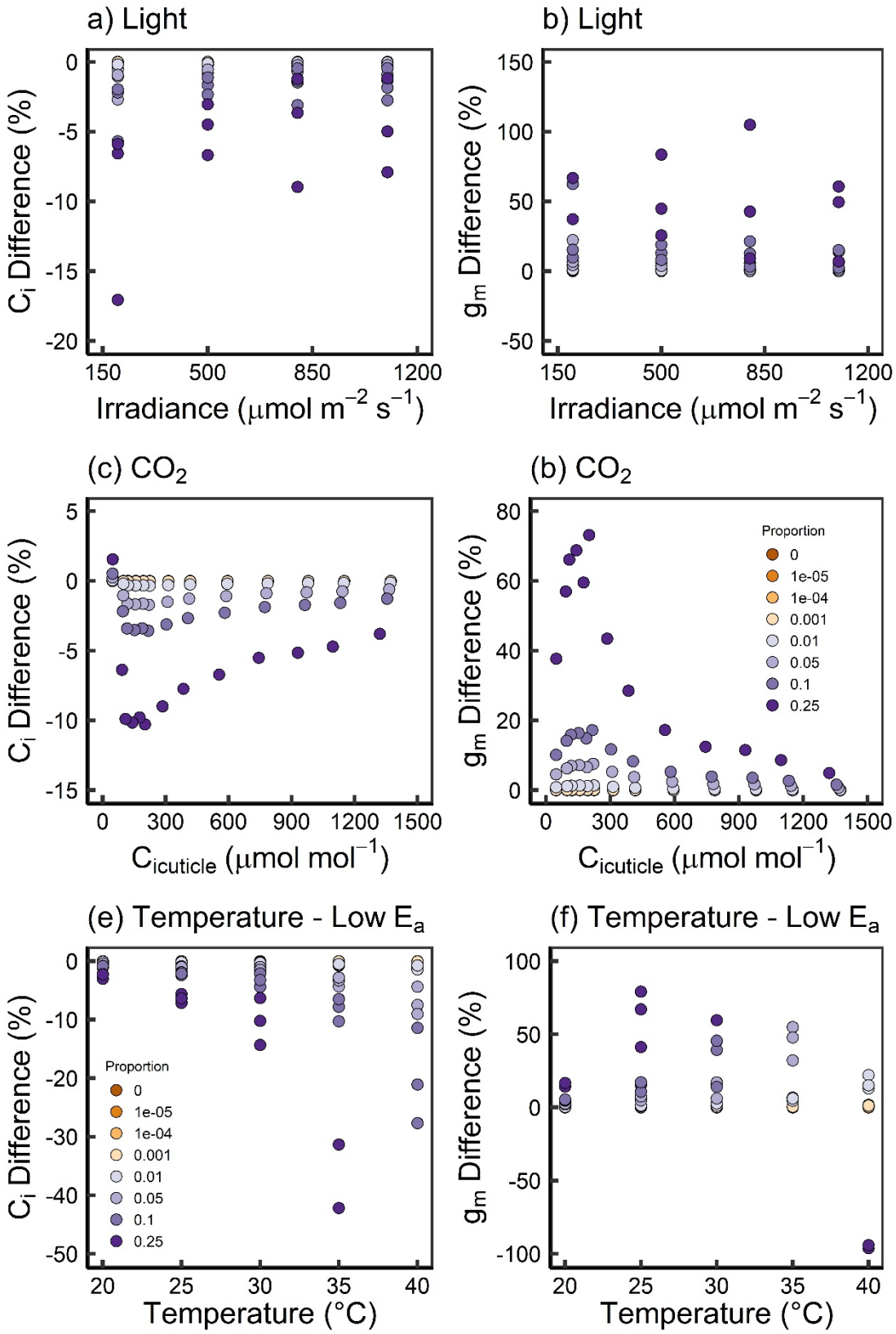

Figure 4

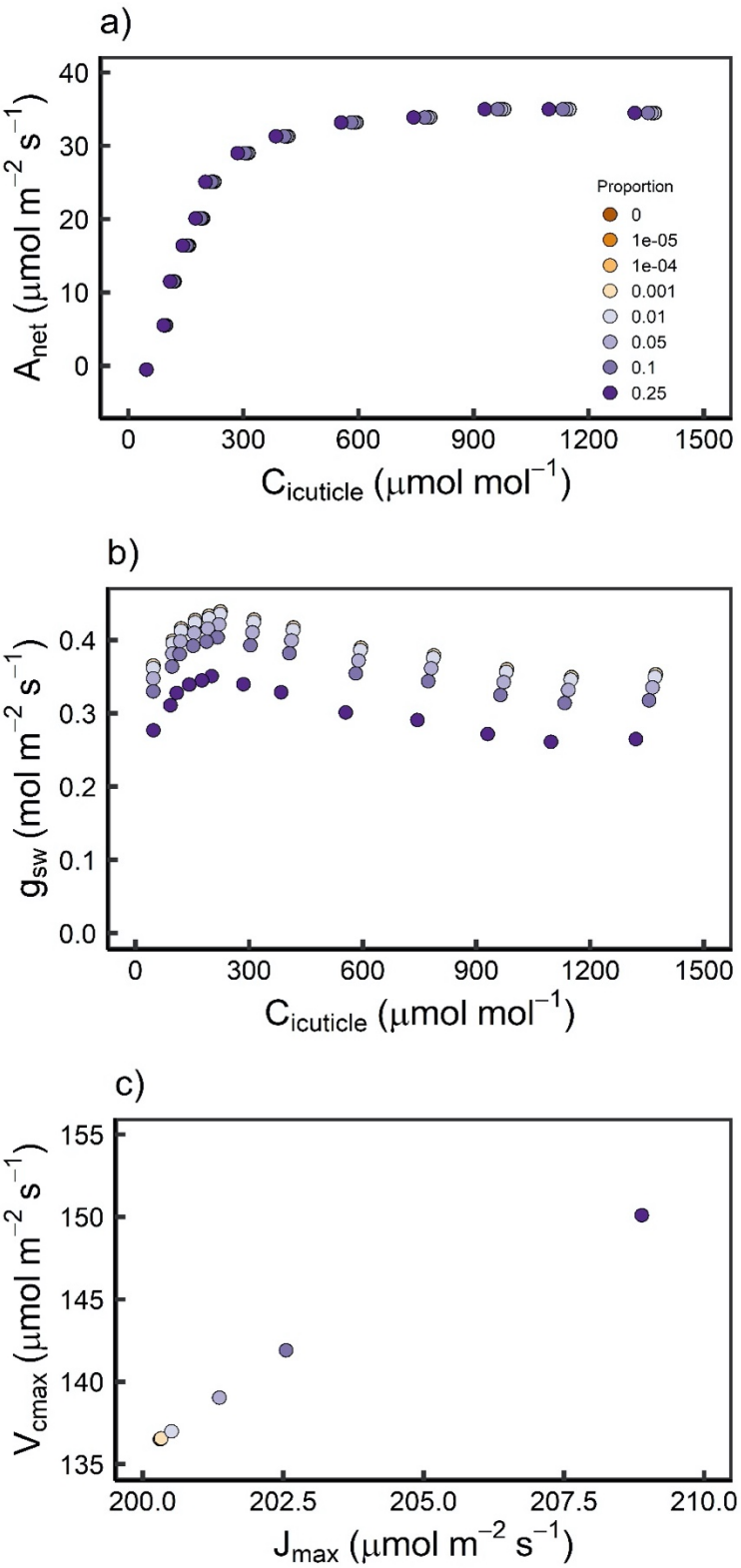

Figure 5

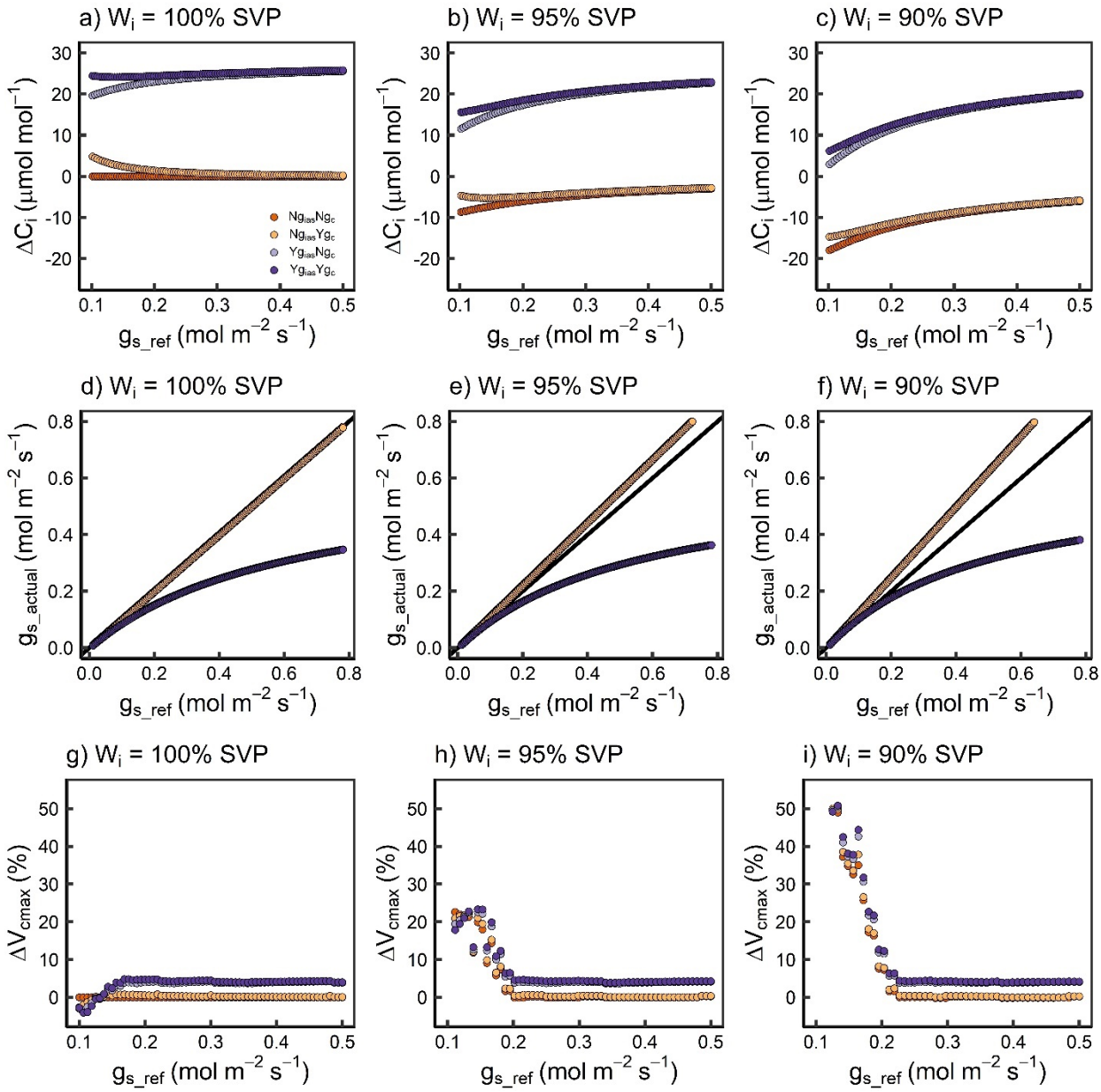

Figure 6

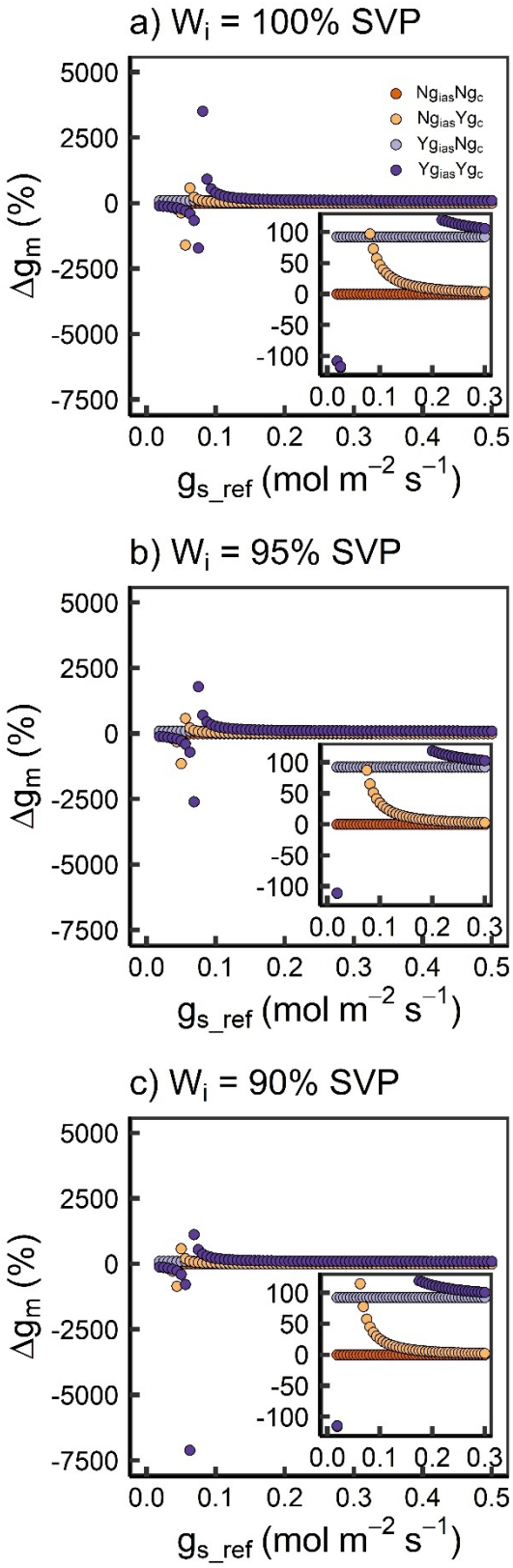

Figure 7

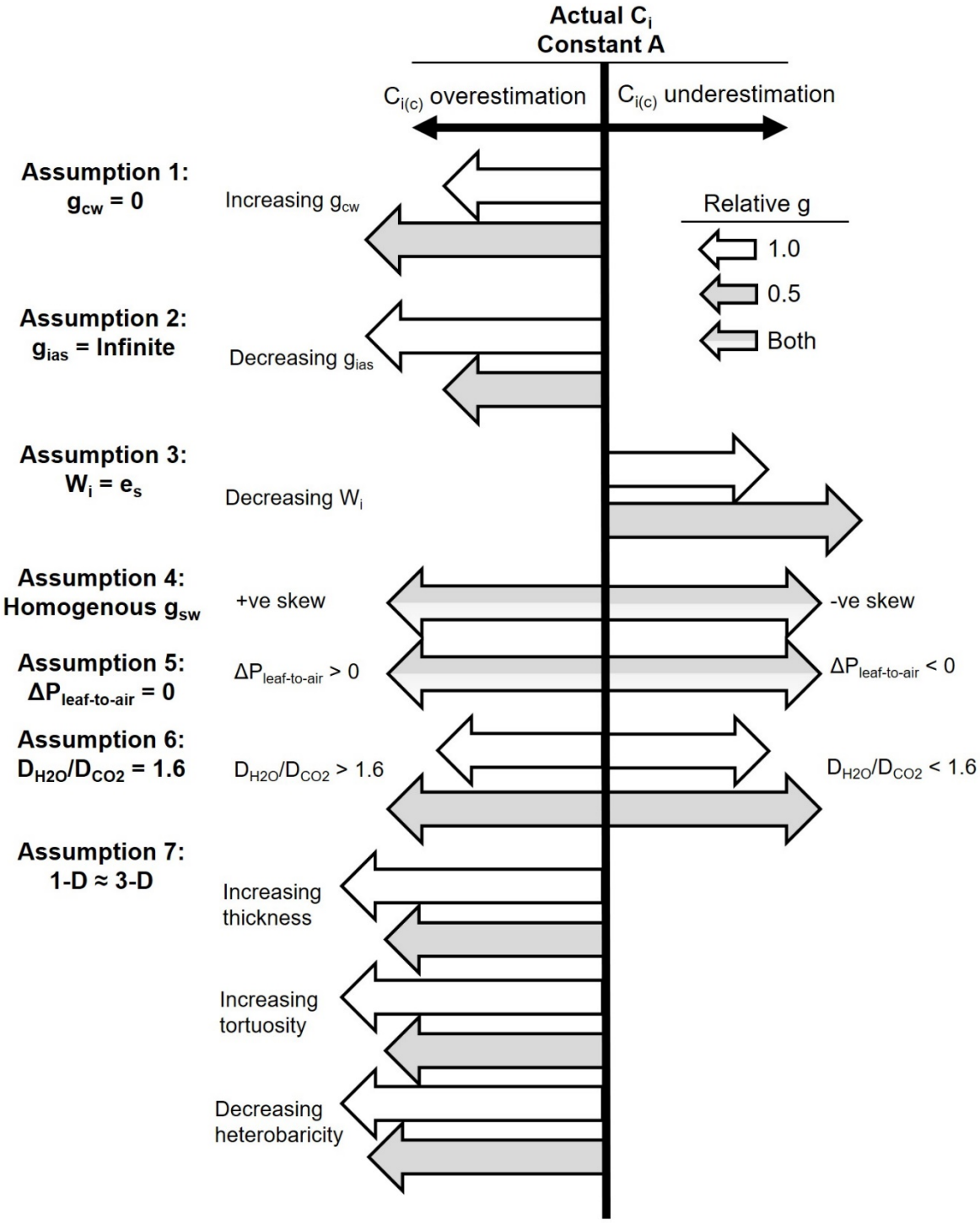

Figure 8

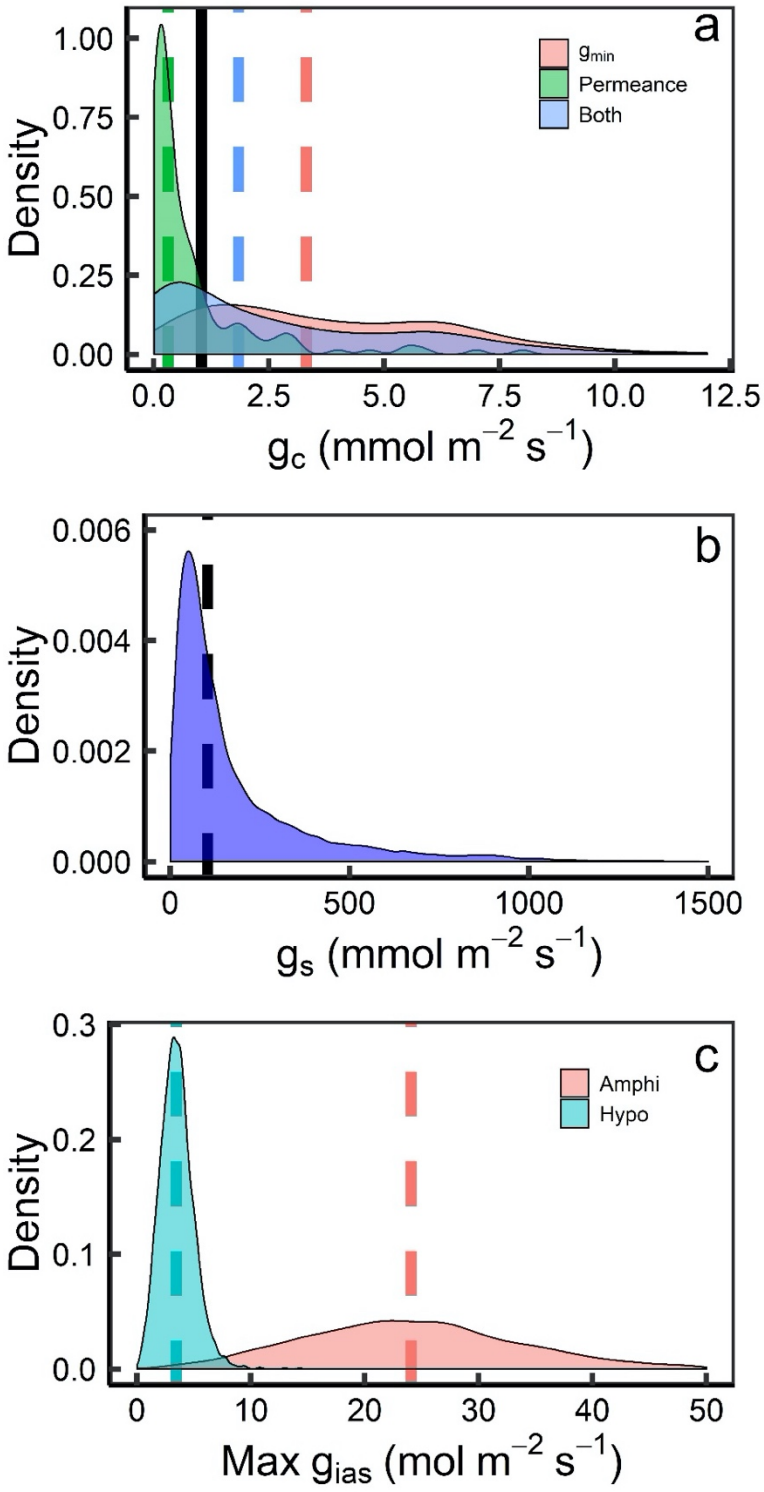

Figure 1

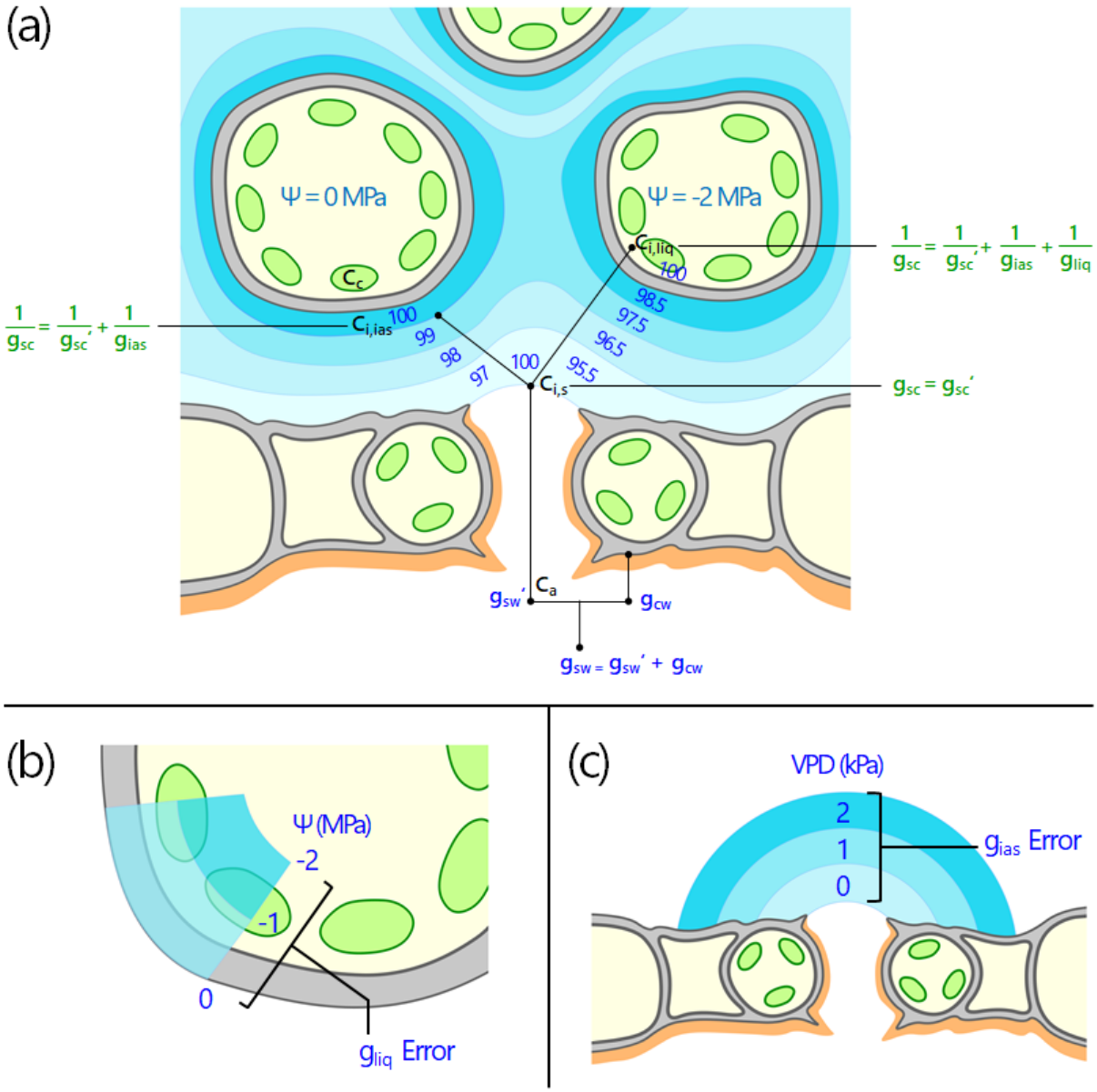

Figure 2

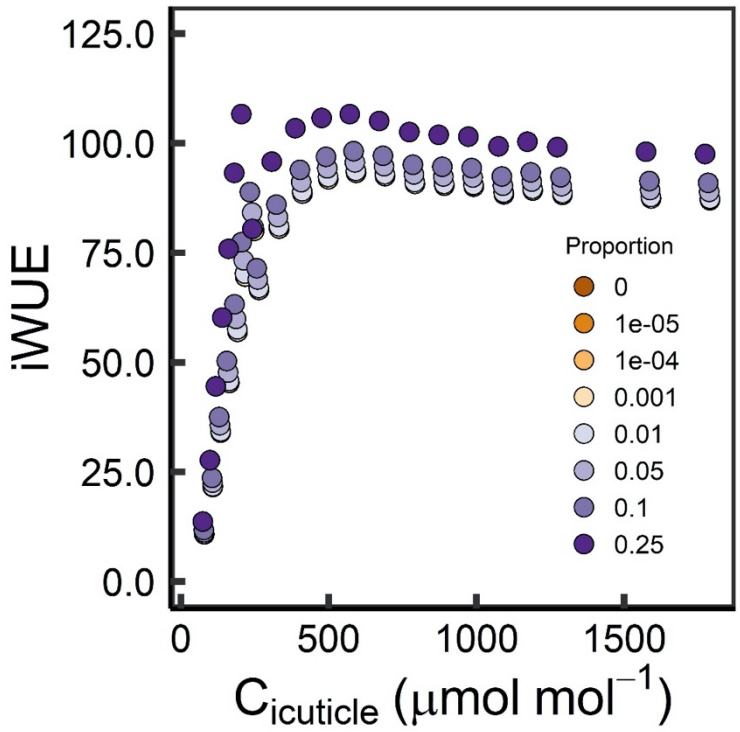

Figure 3

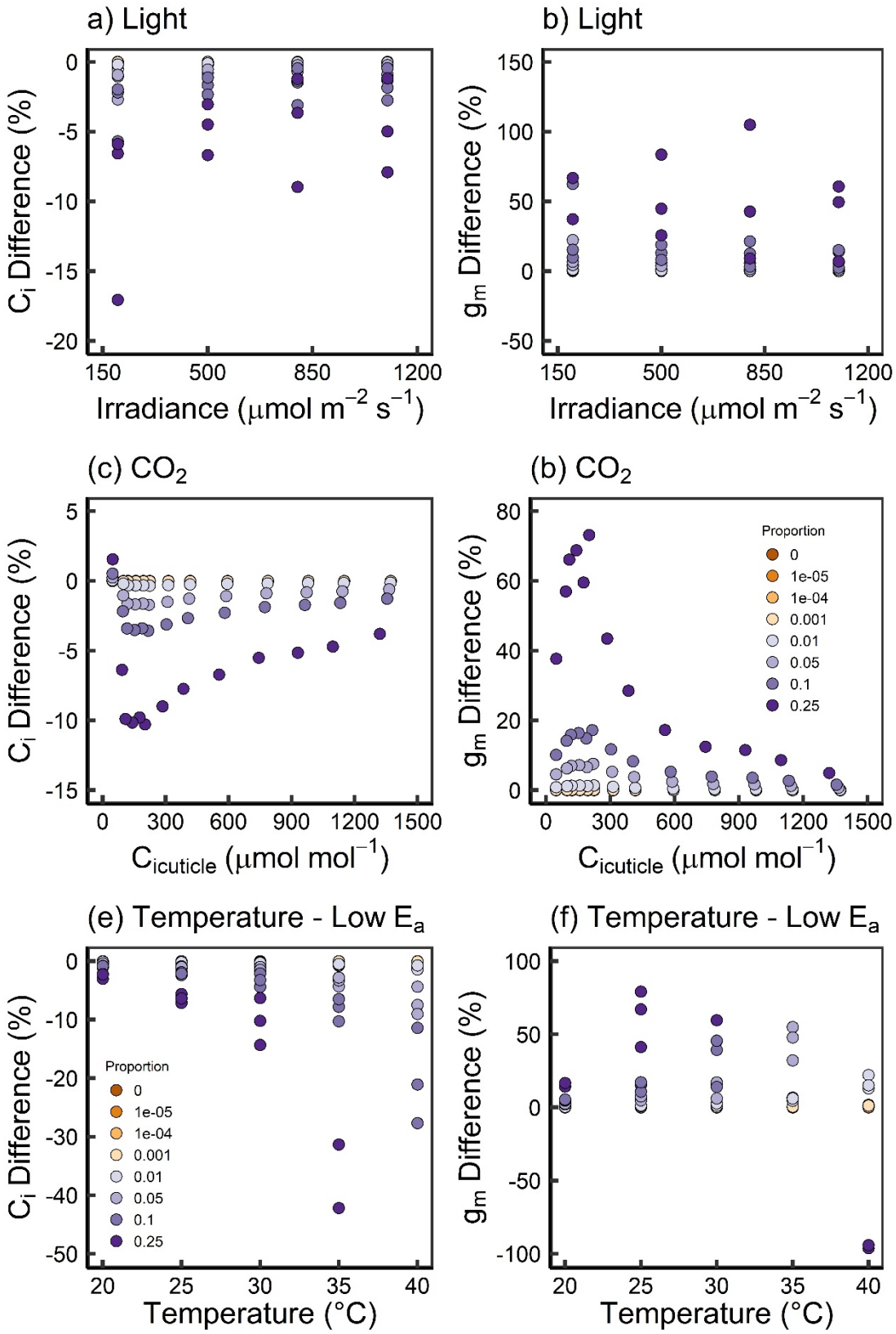

Figure 4

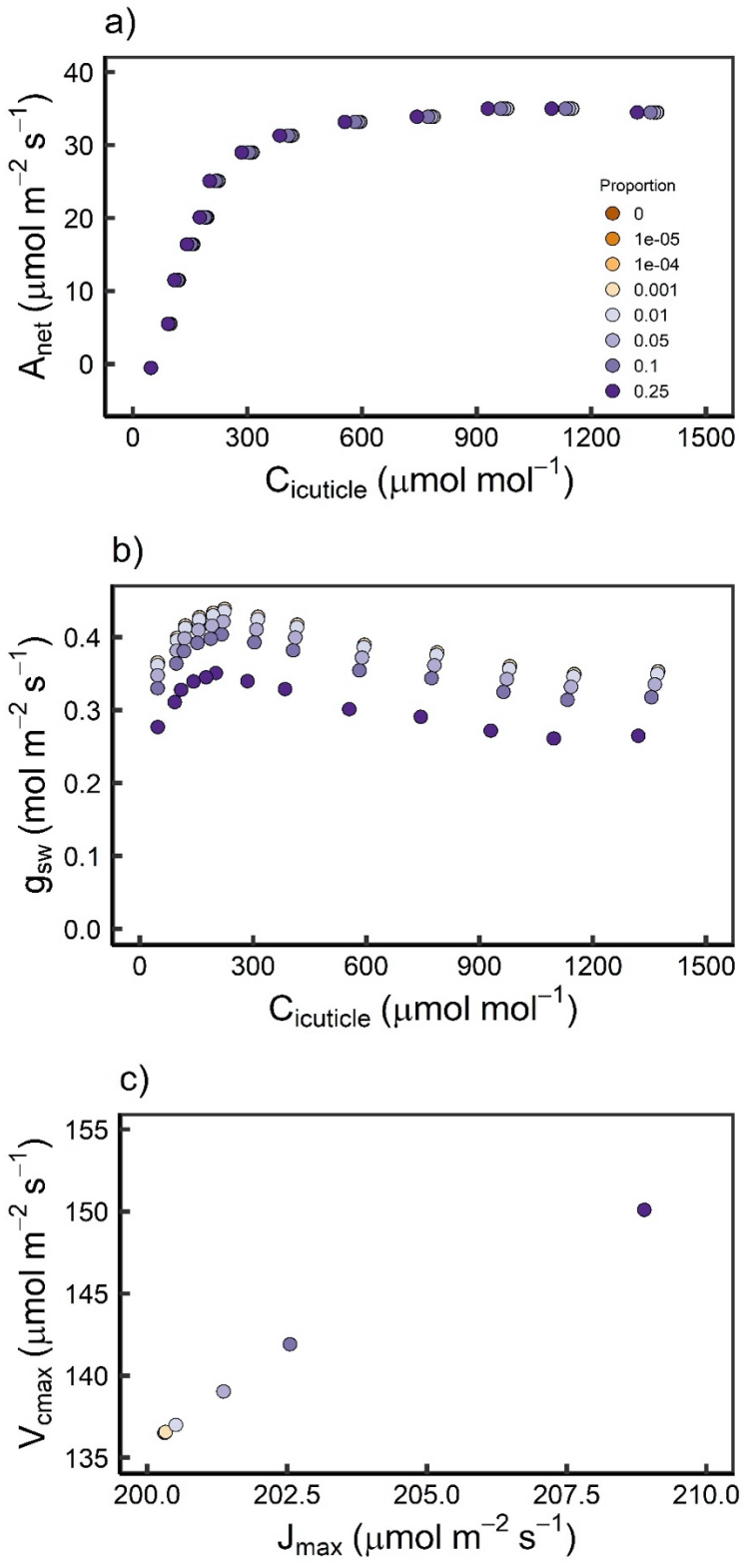

Figure 5

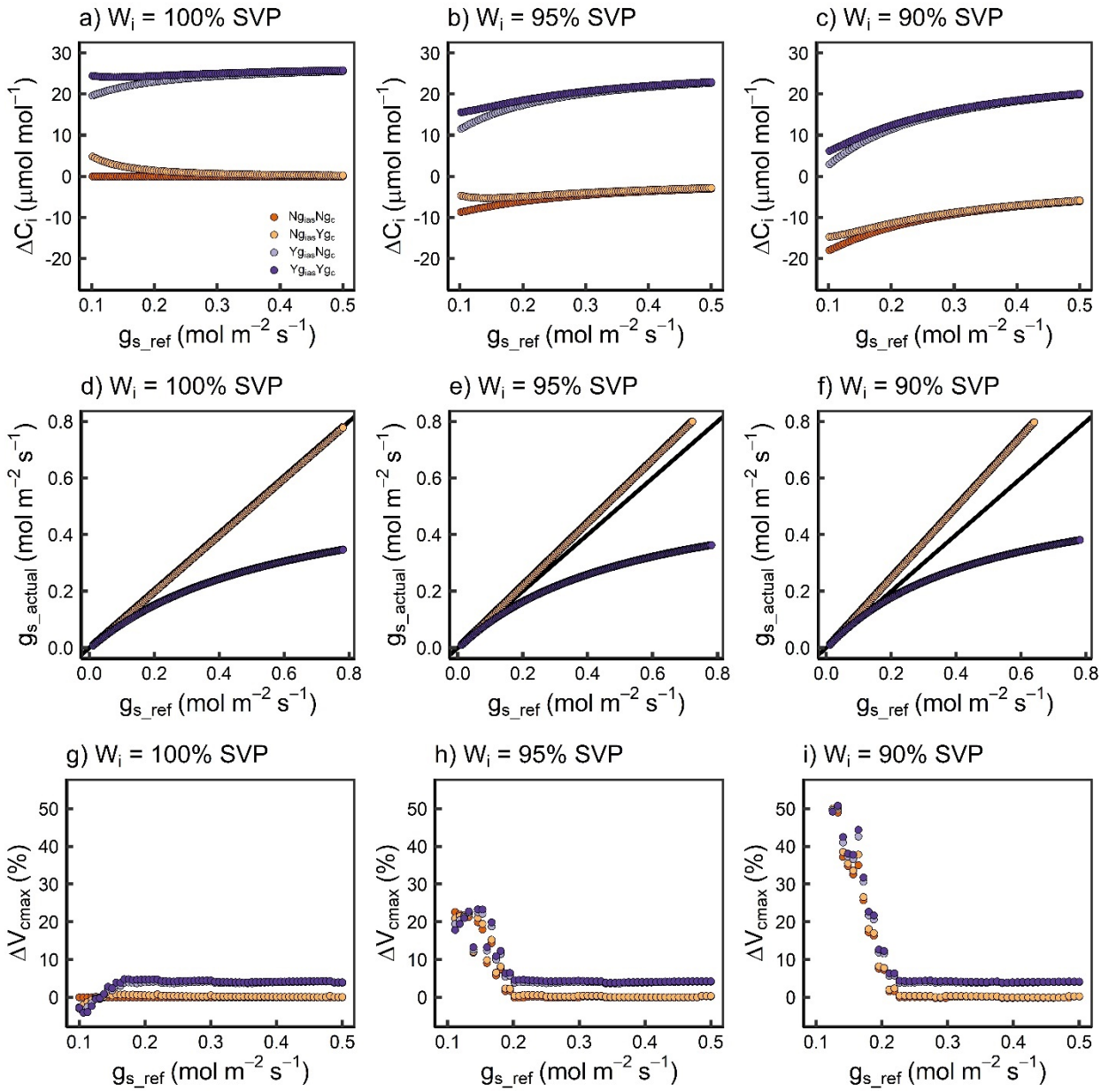

Figure 6

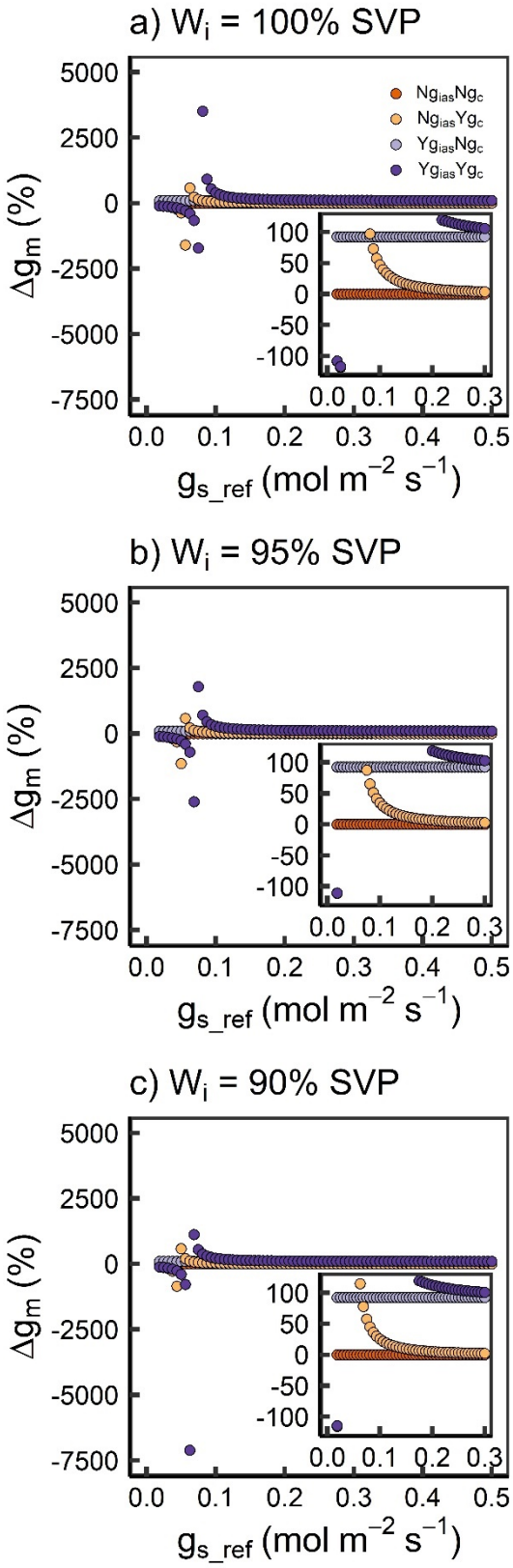

Figure 7

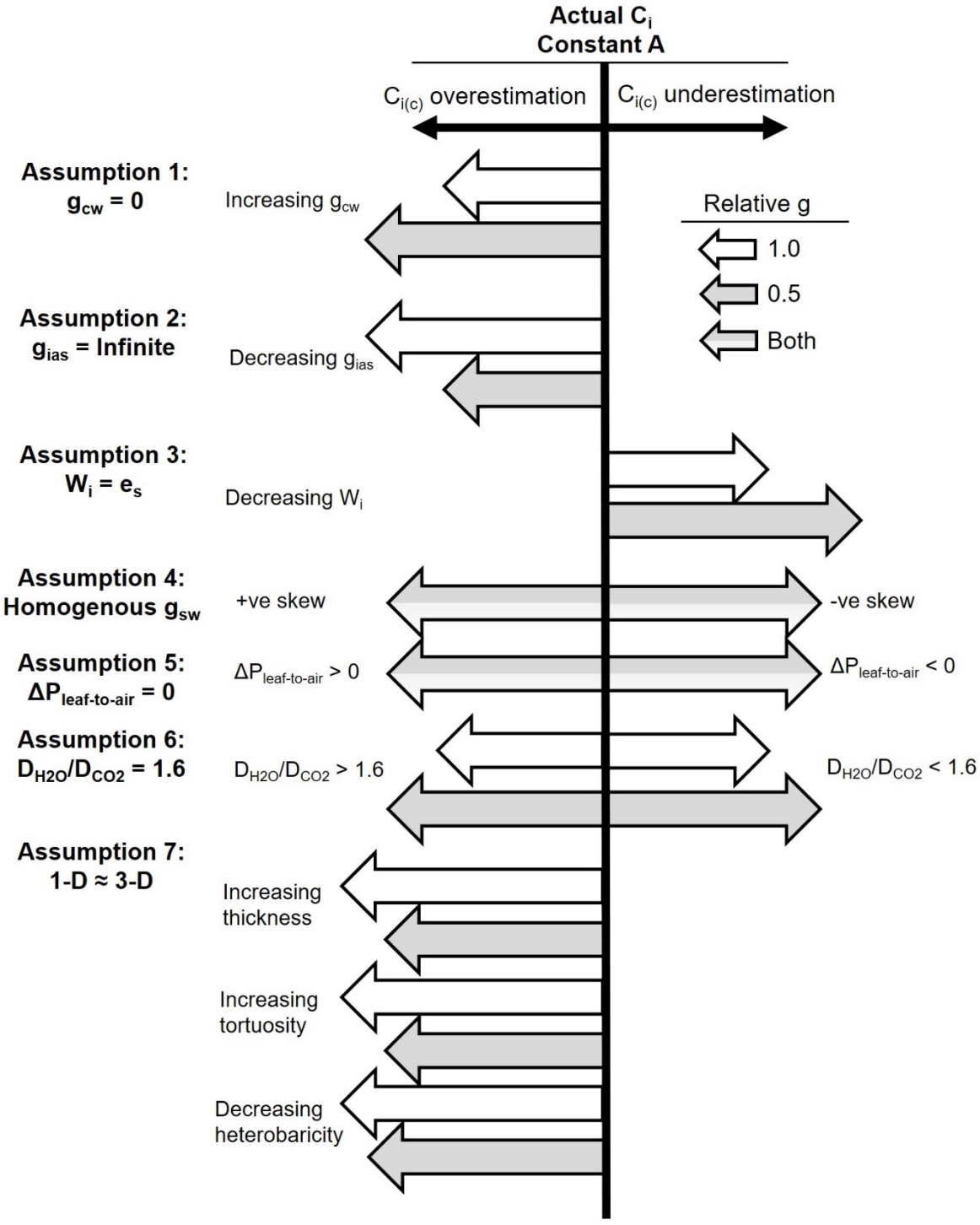

Figure 8